

**Protein Dynamics and Inhibition of 3-Deoxy-
arabino-heptulosonate-7-phosphate Synthase**
(DAHPS)

Mandeep Marway, B. Tech.

Department of Chemistry and Chemical Biology, McMaster University

In partial fulfillment of the requirements for the degree Master of Science

McMaster University

© Copyright by Mandeep Marway, December 2019

Abstract

Antibiotic resistance is the ability of microorganisms to overcome the effects of an antibiotic. While the development of antibiotic resistance is a natural process, the overuse and misuse of antibiotics is accelerating it dramatically. It is estimated that by the year 2050, antibiotic resistance will claim 10 million lives per year unless new therapies are developed. The shikimate pathway is an attractive target for antibiotic development as it is found in archaea, bacteria, fungi and plants, but not in mammals. It begins with the condensation of phosphoenolpyruvate and erythrose 4-phosphate in an aldol-like reaction to produce 3-deoxy-*arabino*-heptulosonate-7-phosphate (DAHP), catalyzed by DAHP synthase (DAHPS). The pathway leads to the aromatic amino acids, phenylalanine, tryptophan, and tyrosine, and a variety of other aromatic compounds. Our lab has previously produced and characterized potent oxime-based inhibitors of DAHPS and the related enzymes KDO8P synthase and NeuB, an *N*-acetylneuraminate synthase. The DAHPS·DAHP oxime crystal structure showed half-of-sites inhibitor binding to this homotetrameric enzyme, consistent with the residual enzyme activity observed at high inhibitor concentrations. The crystal structures offered no explanation of the half-of-sites binding, showing minimal changes upon inhibitor binding. However, global hydrogen-deuterium exchange revealed large differences in protein dynamics in the presence and absence of substrates and inhibitors. Our lab is working on understanding the protein dynamics of tyrosine-regulated DAHPS to understand its function and inhibition. Recently, it has been

difficult to produce active enzyme, though a number of improvements to the procedure have been developed. In addition, new inhibitory motifs were developed for phenylalanine-regulated DAHPS. This includes *N*-formylhydrazone-based inhibitor fragments. Pyruvate *N*-formylhydrazone showed inhibitor activity with $K_i = 11 \pm 3 \mu\text{M}$ and $K_i = 6 \pm 3 \mu\text{M}$ in the presence of glycerol 3-phosphate, indicating that glycerol 3-phosphate occupying the distal end of the active site helps improve inhibitor binding. This molecule will be further characterized, then the full-size DAHP-based inhibitor will be synthesized and characterized.

Acknowledgements

I would like to thank my supervisor, Dr. Paul Berti, for giving me this once-in-a-lifetime opportunity to grow and learn through this project. Thank you for all the help and support you have provided me over the past couple of years. I would also like to thank my committee members, Dr. Giuseppe Melacini and Dr. Paul Harrison, for all the productive criticism and recommendations during my committee meetings.

Additionally, I would like to thank the Berti lab group, Chen Niu, Pallavi Mukherjee, Rebecca Turner, Klara Stringa, Lovette Chan, Victoria Brown, Jessica Mo, Vanessa DiCecco, James Anupol, Claire Willmer, Shahbano Syed, Chris McChesney, and Sabih Jamil. It was a great honour to have worked with such a great group of individuals. Thank you for making this experience that much more exciting and pleasant.

Finally, I would like to thank my family and close friends for always being there to motivate and support me. I would not be where I am without your love and encouragement.

Table of Contents

Abstract	ii
Acknowledgements	iv
Table of Contents	v
List of Figures	viii
List of Tables	x
List of Abbreviations	xi
1. Introduction	1
1.1. Overview	1
1.1.1. Antibiotic Resistance	1
1.1.2. The Shikimate Pathway and DAHP Synthase	2
1.1.3. DAHPS Structure and Function.....	4
1.2. Protein Dynamics	6
1.2.1. Hydrogen-Deuterium Exchange (HDX) and Protein Dynamics	7
1.2.2. Protein Dynamics and DAHP Synthase	8
1.2.3. Summary of Protein Dynamics of DAHP Synthase	10
1.3. Methods of characterizing protein solubility and stability.....	11
1.3.1. Dynamic Light Scattering (DLS).....	11
1.3.2. Methods to Prevent Aggregation	13
1.4. Inhibitor Design.....	14
1.4.1. Fragment-Based Inhibitor Design.....	14
1.4.2. Inhibitor Design with DAHP Oxime and DAHP Hydrazone	15
1.4.3. Summary of Inhibitor Design	19
2. Materials and Methods	20
2.1. Materials.....	20
2.1.1. General.....	20
2.2. Protein production, purification and characterization	20
2.2.1. Production of Electrocompetent Cells	20
2.2.2. Production of Chemically Competent Cells	21
2.2.3. Plasmid Transformation using Electroporation	21

2.2.4. Plasmid Transformation using Heat-Shock	21
2.2.5. DAHPS(Y) Expression and Purification	22
2.2.6. DAHPS(F) Expression and Purification	23
2.2.7. TEV Protease Expression and Purification.....	23
2.2.8. Plasmid Sequencing.....	24
2.2.9. Dynamic Light Scattering (DLS).....	24
2.2.10. Rate assays using Malachite Green/ammonium molybdate (MG/AM) detection	24
2.2.11. Synthesis and Purification of Erythrose-4-Phosphate (E4P)	25
2.2.12. Alkaline Phosphatase (APase) Assay	25
2.3. Inhibitor Synthesis and Testing.....	26
2.3.1. Lactate dehydrogenase (LDH) assay	26
2.3.2. Pyruvate-N-Formylhydrazone (PFH) Synthesis.....	26
2.3.3. Inhibitory Testing of PFH using the MG/AM Assay	27
2.3.4. DAHP Synthesis	27
2.3.5. Pyruvate Oxime Synthesis.....	28
3. Results.....	29
3.1. Protein Dynamics	29
3.1.1. Expression and Purification of DAHPS(Y).....	29
3.1.2. Troubleshooting DAHPS(Y) production.....	31
3.1.3. Unexpected Antibiotic Resistance of E. coli BL21(DE3) cells.....	44
3.2. Inhibitor Design.....	46
3.2.1. Pyruvate Formylhydrazone (PFH).....	46
3.2.2. Inhibitory Assays with PFH using MG/AM Assay	49
3.2.3. DAHP Synthesis and Purification	50
4. Discussion	52
4.1. Protein Dynamics	52
4.1.1. DAHPS(Y) Troubleshooting	52
4.1.2. Troubleshooting Purification Conditions	52
4.1.3. Troubleshooting Expression Conditions.....	54
4.1.4. Aeropyrum pernix DAHPS.....	54

4.2. Inhibitor Design.....	54
4.2.1. PFH Synthesis and Testing.....	54
4.3. Future Directions.....	56
4.3.1. Protein Dynamics.....	56
4.3.2. Inhibitor Design.....	56
5. Appendix.....	58
5.1. Appendix 1 – Mass Spectrum of DAHPS(Y)	58
5.2. Appendix 2: NMR and Mass Spectra for Pyruvate, FAH, and PFH.....	59
5.3. Appendix 3 – Computational prediction of PFH NMR chemical shifts ..	64
5.3.1. Summary	64
5.3.2. Rationale	65
5.3.3. Chemical shift trends	68
5.3.4. Predicted chemical shifts (ppm)	68
5.3.5. Predicted peak positions	70
References	72

List of Figures

Figure 1: The DAHPS-catalyzed reaction.	2
Figure 2: The seven steps of the shikimate pathway	3
Figure 3: The chorismate branchpoint in the shikimate pathway	3
Figure 4: Crystal structure of DAHPS·PEP·Co ²⁺ ·G3P	5
Figure 5: DAHPS(F)·DAHP oxime crystal structure.	5
Figure 6: Hydrogen/deuterium exchange protocol.	7
Figure 7: Model of DAHPS(Y) monomer, based on DAHPS(F).	9
Figure 8: ¹⁹ F NMR spectra of F-Trp labelled DAHPS(Y).	10
Figure 9: Schematic of a DLS spectrometer.	12
Figure 10: Example DLS spectra.	12
Figure 11: Workflow of fragment-based drug discovery (FBDD).	15
Figure 12: DAHP oxime and pyruvate oxime.	16
Figure 13: DAHP Hydrazone to Pyruvate Hydrazone (fragment).	16
Figure 14: DAHPS(F)·DAHP hydrazone structure.	17
Figure 15: Pyruvate hydrazone to Pyruvate- <i>N</i> -formylhydrazone	17
Figure 16: Pyruvate oxime to <i>N</i> -hydroxyalanine.	18
Figure 17: DAHPS(Y) Purification.	29
Figure 18: DAHPS(F) Purification.	30
Figure 19: DAHPS(F) activity in the presence of variable EDTA concentrations.	31
Figure 20: E4P Synthesis	32
Figure 21: E4P dimer.	33
Figure 22: DLS on untreated DAHPS(Y).	35
Figure 23: DLS on DAHPS(Y) treated with 1mM MgCl ₂	36
Figure 24: DLS on DAHPS(Y) treated with 1mM TCEP.	37
Figure 25: DLS on DAHPS(Y) treated with 1mM MgCl ₂ and 1mM TCEP.	38
Figure 26: DLS on DAHPS(Y) treated with 50mM Arginine + 50mM Glutamic Acid.	40
Figure 27: DLS on different purification methods.	42

Figure 28: DLS of DAHPS(Y) vs. DAHPS(F).....	44
Figure 29: DAHPS(Y) expressed at 37°C with IPTG.....	45
Figure 30: DAHPS from <i>Aeropyrum pernix</i> (<i>A. pernix</i>) expressed at 37°C with IPTG.....	45
Figure 31: Possible <i>E</i> and <i>Z</i> isomers of PFH.	48
Figure 32: PFH inhibition of DAHPS(F).....	50
Figure 33: Pi(nmol) vs. Aliquot Size (10x dilution) for DAHP	51
Figure 34: Mass spectrum of DAHPS(Y).....	58
Figure 35: ¹ H-NMR for pyruvate acquired using the 600MHz NMR.	59
Figure 36: ¹ H-NMR for FAH acquired using the 600MHz NMR.	59
Figure 37: ¹ H-NMR for crude Pyruvate- <i>N</i> -Formylhydrazone (PFH) acquired using the 600MHz NMR.....	60
Figure 38: High-Resolution MS for crude PFH.....	61
Figure 39: ¹ H-NMR for purified Pyruvate- <i>N</i> -Formylhydrazone (PFH) acquired using the 600MHz NMR.....	61
Figure 40: ¹³ C-NMR for purified Pyruvate- <i>N</i> -Formylhydrazone (PFH) acquired using the 600MHz NMR.....	62
Figure 41: HMBC NMR for purified Pyruvate- <i>N</i> -Formylhydrazone (PFH) acquired using the 600MHz NMR.	62
Figure 42: HSQC NMR for purified Pyruvate- <i>N</i> -Formylhydrazone (PFH) acquired using the 600MHz NMR.	63
Figure 43: High-Resolution MS for purified PFH.....	63
Figure 44: 8 possible isomers characterized using quantum mechanical optimizations.....	67

List of Tables

Table 1: Tabulated results for MS for crude PFH..... 61

Table 2: Tabulated results for MS for purified PFH..... 64

List of Abbreviations

APase	Alkaline Phosphatase
CALB	<i>Candida antarctica</i> Lipase B
DAHP	3-deoxy-D- <i>arabino</i> -heptulosonate-7-phosphate
DAHPS	DAHP synthase
DLS	Dynamic Light Scattering
DMSO	Dimethyl sulphoxide
E4P	Erythrose-4-Phosphate
FAH	Formic acid hydrazide
FBDD	Fragment-based drug discovery
G3P	Glyceraldehyde-3-phosphate
G6P	Glucose-6-phosphate
G6PDH	Glucose-6-phosphate dehydrogenase
Gro3P	Glycerol-3-phosphate
HDX	Hydrogen-Deuterium Exchange
HMBC	Heteronuclear Multiple Bond Correlation
HSQC	Heteronuclear Single Quantum Coherence
IPTG	Isopropyl- β -D-thiogalactopyranoside
KDO8P	3-deoxy-D- <i>manno</i> -2-octulosonate-8-phosphate
LDH	Lactate dehydrogenase
MG/AM	Malachite green/ammonium molybdate
MS	Mass spectrometry

NMR	Nuclear magnetic resonance
PEP	Phosphoenolpyruvate
PFH	Pyruvate- <i>N</i> -formylhydrazone
P _i	Inorganic phosphate
PIC	Protease inhibitor cocktail
RSA	Reducing sugar assay
TCEP	Tris (2-carboxyethyl) phosphine
TEV protease	Tobacco etch virus protease

1. Introduction

1.1. Overview

1.1.1. Antibiotic Resistance

Antibiotic resistance is the ability of microorganisms to overcome the effects of an antibiotic¹. While the development of antibiotic resistance is a natural process, the overuse and misuse of antibiotics is accelerating it dramatically. It is estimated that by the year 2050, antibiotic resistance will claim 10 million more lives per year than currently unless new therapies and targets are investigated². The shikimate pathway is an attractive target for antibiotic development as it is found in archaea, bacteria, fungi and plants, but not in mammals³. It begins with the condensation of phosphoenolpyruvate (PEP) and erythrose 4-phosphate (E4P) in an aldol-like reaction to produce 3-deoxy-*arabino*-heptulosonate-7-phosphate (DAHP), catalyzed by DAHP synthase (DAHPS)³. The pathway leads to the aromatic amino acids, phenylalanine, tryptophan, and tyrosine, and a variety of other aromatic compounds. Our lab is working on understanding the protein dynamics and inhibition of DAHPS^{4,5}. Recently, it has been difficult to produce active *Escherichia coli* DAHPS(Y), the tyrosine-regulated isozyme. A number of improvements to the procedure were developed to address this problem. In addition, new inhibitory motifs are being developed for phenylalanine-regulated DAHPS. This includes *N*-formylhydrazone-based inhibitor fragments. These molecules are currently being further characterized in order to synthesize the full-size DAHP-based inhibitors for characterization and co-crystallization with DAHPS.

1.1.2. The Shikimate Pathway and DAHP Synthase

The shikimate pathway is one potential target for antibiotic development. It uses seven enzymes to convert PEP and E4P to chorismate³. The pathway begins with the condensation reaction of PEP and E4P in an aldol-like reaction to produce DAHP, catalyzed by DAHPS (Figure 1)⁶.

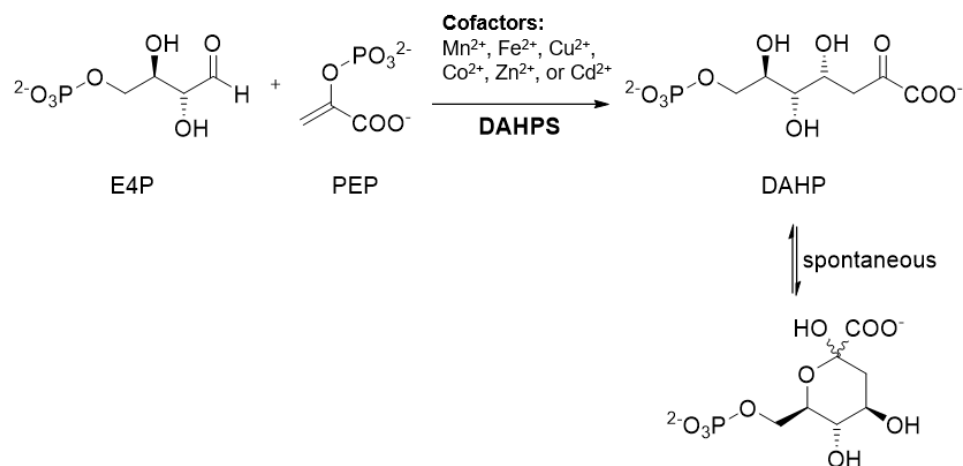


Figure 1: The DAHPS-catalyzed reaction.

DAHPS is divalent metal-ion dependent. Several metal ions have been proposed as the essential activator *in vivo*⁷, though non-physiological ions, including Mn²⁺ and Cd²⁺ also activate the enzyme⁷. (Figure created by Dr. Berti.)

DAHP then enters the shikimate pathway, ending with chorismate (Figure 2)⁸, at which point the pathway diverges.

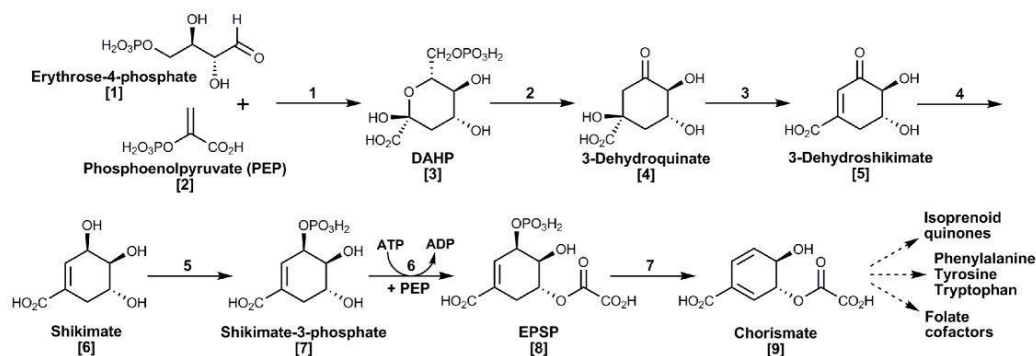


Figure 2: The seven steps of the shikimate pathway

Enzymes: 1) 3-deoxy-*arabino*-heptulosonate-7-phosphate synthase (DAHPS), 2) 3-dehydroquininate synthase (DHQ synthase), 3) 3-dehydroquininate dehydratase (DH-quinase), 4) shikimate dehydrogenase (Shikimate DH), 5) shikimate kinase (SKI), 6) 5-enolpyruvylshikimate-3-phosphate synthase (EPSP), 7) chorismate synthase⁸.

Chorismate is then used to produce aromatic amino acids, folate cofactors and isoprenoid quinones⁸ (Figure 3)⁶.

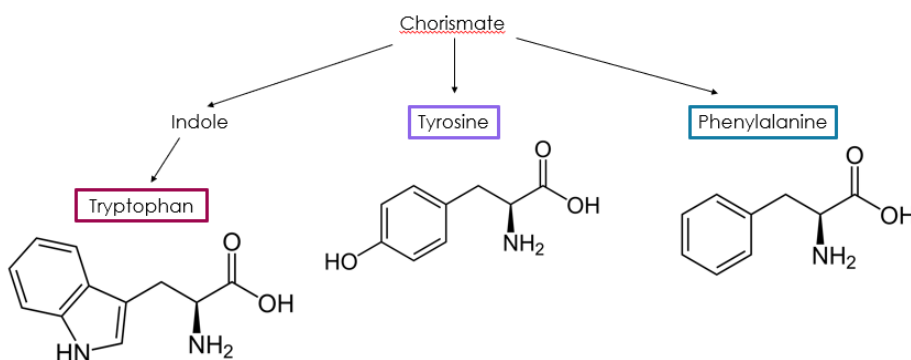


Figure 3: The chorismate branchpoint in the shikimate pathway

The shikimate pathway follows a common pathway up to chorismate, at which point it diverges into separate pathways leading to each aromatic amino acid⁸.

DAHPS is essential for bacterial virulence⁹ and occurs in all bacteria, archaea, fungi, and plants, but is not found in humans or other mammals^{3,10}, making it a viable target for broad-spectrum antibiotics¹¹. *E. coli* produces three DAHPS isozymes. Most of the activity is from the DAHPS(F) isozyme, which is subject to feedback inhibition by phenylalanine, and is a homotetramer. DAHPS(Y) and DAHPS (W) are feedback inhibited by tyrosine and tryptophan, respectively, and are homodimers¹².

Based on this knowledge, it is believed that by inhibiting the function of DAHPS, the production of these amino acids can be prevented, thus limiting growth of the organism.

1.1.3. DAHPS Structure and Function

DAHPS is part of the NeuB superfamily of α -carboxyketose synthases, which is a superfamily of enzymes which are currently under study as antimicrobial targets⁴. Other enzymes in this family include 3-deoxy-D-manno-2-octulosonate-8-phosphate (KDO8P) synthase, which is responsible for the synthesis of KDO residues, one component of lipopolysaccharide¹³. NeuB is found in neuro-invasive bacteria that use its product, *N*-acetylneuraminate, to evade the immune system¹⁴.

The crystal structure of *Saccharomyces cerevisiae* DAHPS(Y) revealed the PEP (red), Co^{2+} (gray) and glyceraldehyde-3-phosphate (G3P) (yellow) binding sites (Figure 4). G3P was used as an E4P mimic because it lacks the reactive carbonyl group that would lead to the chemical reaction in DAHPS to be triggered¹⁵. DAHPS is divalent metal ion dependent, and the type of metal ion used has an influence on the k_{cat} and the apparent E4P affinity¹⁵.

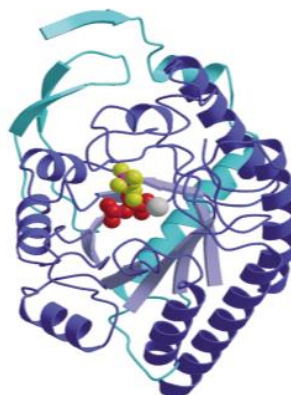


Figure 4: Crystal structure of DAHPS·PEP·Co²⁺·G3P

S. cerevisiae DAHPS is a homotetrameric enzyme with a TIM barrel (α/β)₈ protein fold¹⁶. The active site is located at the C-end of the β -barrel¹⁶. The ligands are shown as sphere representations, i.e., Co²⁺ (gray), G3P (yellow), and PEP (red)¹⁵.

DAHPS oxime is an inhibitor that was prepared against DAHPS(F) with a K_i of 1.5 μ M, and a residence time of 83 min, but only partial inhibition, with residual activity even at very high substrate concentrations⁴. DAHPS(F) co-crystallized with the DAHPS oxime in the absence of substrates had inhibitor bound only to two subunits of the homotetrameric protein, and showed minimal structural changes when the inhibitor was bound⁴ (Figure 5).

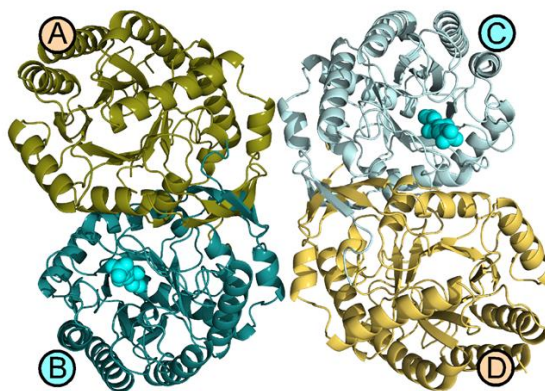


Figure 5: DAHPS(F)·DAHPS oxime crystal structure.

DAHPS(F) was co-crystallized with DAHP oxime⁴. The biologically active form is the homotetramer, composed of a dimer-of-dimers quaternary structure. In the crystal structure inhibitor was bound to only one subunit of the tight dimer pair, namely subunit B and C. There were minimal conformational differences between subunits A/D and B/C. (Figure is Figure 6a of reference 4) (PDBID: 5CKS).

DAHP oxime inhibited subunits B and C competitively with respect to the substrates Mn^{2+} , PEP and E4P, and subunits A and D allosterically⁴. At high inhibitor concentrations, when the inhibitor was bound to subunits B and C, $K_{M,E4P}$ in subunits A and D decreased by at least 10-fold⁴. Based on this, it is clear that there is a communication between the subunits in DAHPS(F) with respect to ligand binding.

1.2. Protein Dynamics

Protein dynamics is the study of how protein flexibility affects function^{17,18}. It is often possible to infer aspects of protein function from their crystal structures, which are inherently static pictures. However, in reality, proteins in solution undergo constant conformational change, with different peptides displaying widely differing flexibilities, i.e., rates of conformational change. Protein dynamics is the study of these ensembles of protein conformations, and their flexibility, and how those affect protein function. It is critical to understanding protein function¹⁷, and protein structure is essential for protein dynamics and function¹⁸. Function is the end result of the 3-D structure, which can be determined with the help of X-ray crystallography and NMR, and the protein dynamics¹⁹. Understanding protein dynamics is critical to protein and ligand design, as well as ligand and inhibitor binding. Therefore, by understanding enzyme dynamics, understanding functionality and how to inhibit it becomes easier²⁰.

1.2.1. Hydrogen-Deuterium Exchange (HDX) and Protein Dynamics

Given the lack of significant conformational changes between inhibitor-bound and -unbound subunits in the DAHPS(F)·DAHP oxime crystal structure, global hydrogen-deuterium exchange (HDX) experiments were used to probe protein dynamics²¹. HDX works by diluting the protein of interest into a D₂O-containing buffer, allowing exchangeable protons to exchange with deuterons for a defined time, then measuring the extent of exchange by following the increase in mass of the whole protein by mass spectrometry (MS). More dynamic regions undergo the HDX on a millisecond to second time scale, while exchange in more structured (less dynamic) regions can take minutes to months (Figure 6, top). It is also possible to perform spatially-resolved HDX by quenching the exchange reaction at pH 2.5, digesting the protein of interest with an acid-stable protease like pepsin, and measuring the change in mass of individual peptides²².

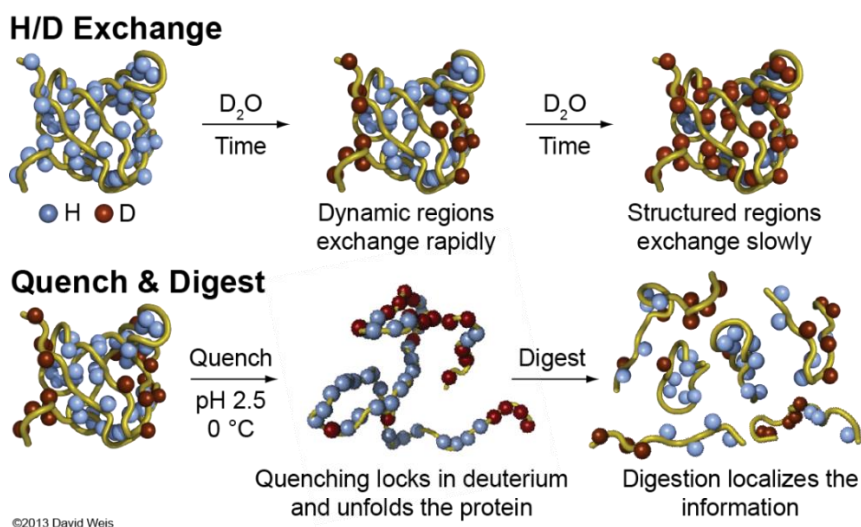


Figure 6: Hydrogen/deuterium exchange protocol.

(top) In global HDX experiments, the whole protein is allowed to undergo H/D exchange for a defined time, then the mass of the whole protein is measured. (bottom) In spatially-resolved HDX

experiments, exchange is quenched at low pH, the protein digested with a protease, and the masses of individual peptides determined by mass spectrometry. (Figure from <https://mvsc.ku.edu/content/hydrogen-deuterium-exchange-mass-spectrometry>.)

Spatially-resolved HDX of DAHPS(F) in the absence of ligands demonstrated an unusual amount of H/D exchange, indicating that the protein is highly dynamic²¹. Adding PEP caused significant changes in protein dynamics, with protein loops near the inter-domain interface becoming more structured (N. Balachandran and D. Wilson, personal communication). Global HDX decreased significantly with the addition of either PEP or DAHP oxime⁴, indicating that the half-of-sites inhibitor binding observed in the crystal structure was due to changes in protein dynamics rather than structure. In addition, we also see that significant parts of the surface of DAHPS(F) are disordered in the absence of ligands compared with crystal structures, all of which have ligands bound in or near the active site²¹. This is further evidence for the importance of protein dynamics to DAHPS's function.

1.2.2. Protein Dynamics and DAHP Synthase

While NMR is frequently used to study protein dynamics, DAHPS(F) is not amenable because of its size (158 kDa for the tetramer). For that reason, DAHPS(Y), a homodimer, would be more tractable. However, a full NMR analysis of the protein would still be challenging due to its size. Hence, we have decided to use ¹⁹F NMR of FTrp-labelled *E. coli* DAHPS(Y). There are only 3 Trp residues in DAHPS(Y), and they are well-located for our purposes. One, W332, is surface-exposed, far from the active site. Another, W105, is on an active site loop containing an Arg residue that forms an ion pair with the phosphate group of E4P/DAHP/DAHP oxime. The equivalent residue in DAHPS(F), W104, is part of the F95–G106 loop which undergoes a large

conformational change upon inhibitor binding⁴. The third Trp residue, W160, is located in the hydrophobic core close to, but not in contact with, the active site (Figure 7).

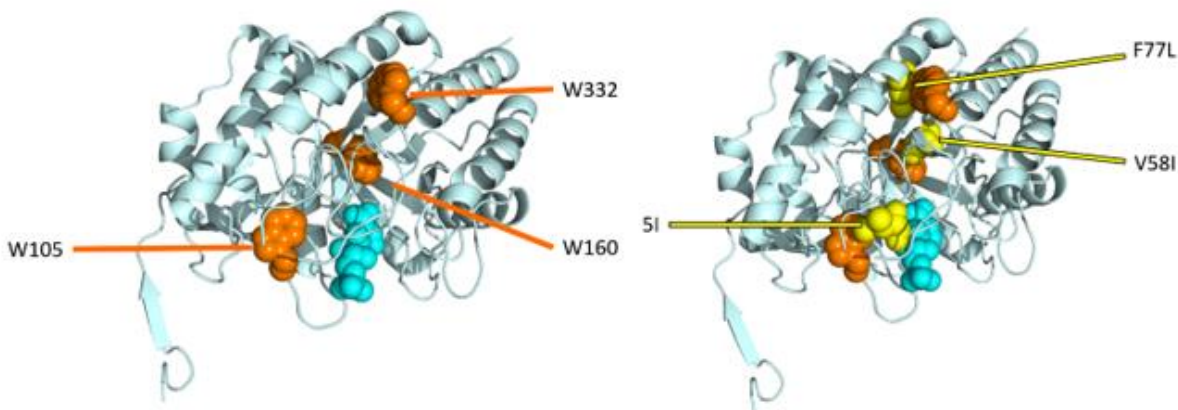


Figure 7: Model of DAHPS(Y) monomer, based on DAHPS(F).

(Left) Shows the Trp residues (orange), and DAHP oxime (cyan) bound in the active site. (Right) Mutating the Trp residues for peak identification led to unstable proteins, so nudge mutations were designed to allow identification of FTrp peaks²³. Nudge mutations are mutations to residues in contact with the Trp residue of interest. The ¹⁹F peak whose position shifts in a nudge mutant corresponds to the Trp residue in contact with the mutated residue. (Figure generated by Dr. Berti.)

Being able to follow protein dynamics via ¹⁹F NMR of FTrp residues would give us a good start to understanding how protein dynamics is involved in DAHPS(Y)'s function. Our lab has previously made FTrp-labelled DAHPS(Y) and found 5 to 6 ¹⁹F peaks under a variety of conditions (Figure 8). If the two subunits were identical, there would be three peaks – one for each FTrp residue in the monomer. The fact that there are 5 to 6 peaks means that the DAHPS(Y), though it is a homodimer, is intrinsically asymmetric in solution (N. Balachandran, S. Larda, and R. S. Prosser, personal communication). This further points to inter-subunit interactions being important for protein function. Some of the ¹⁹F peaks were broad, evidence of

conformational changes on the NMR timescale. The next step was to identify which peaks correspond to each FTrp residue. Mutating each Trp residue to Phe resulted in unstable proteins. The alternative was to design “nudge mutations”²⁴, that is, mutating residues in contact with the Trp residues in order to change their ¹⁹F chemical shift (Figure 7, bottom). These mutations were made by Wayne Law and shown to be stable and soluble, so the next step is to make them in large amounts for NMR. Recently, there have been issues with obtaining active DAHPS(Y), so multiple modifications to the expression and purification protocol have been tested to troubleshoot the cause.

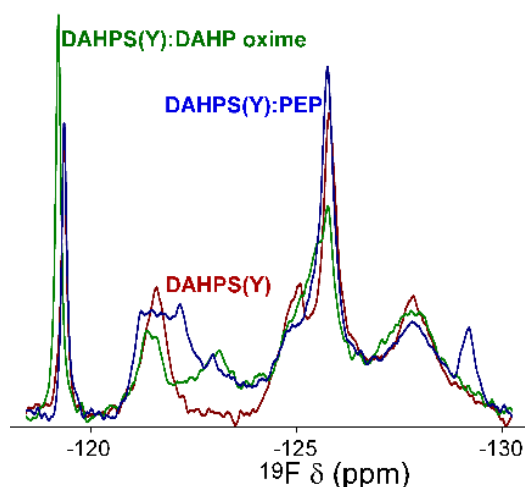


Figure 8: ¹⁹F NMR spectra of F-Trp labelled DAHPS(Y).

¹⁹F NMR spectra of DAHPS(Y) with bound Mg²⁺ (red), PEP (blue), and DAHP oxime (green) were collected. (Figure created by Dr. Berti.)

1.2.3. Summary of Protein Dynamics of DAHP Synthase

The inhibitor, DAHP oxime demonstrated half-of-sites binding, and there were large protein dynamic changes in response to its binding. Because of this change, it is hypothesized

that protein dynamics studies of DAHPS(Y) will lead to a better understanding of its function and inhibition.

1.3. Methods of characterizing protein solubility and stability

DAHPS(Y) proved to be prone to aggregation, precipitation, and inactivation, which affects its suitability for NMR analysis. Dynamic light scattering (DLS) was employed to characterize its solubility and stability.

1.3.1. Dynamic Light Scattering (DLS)

DLS measures particle sizes in solution, so can be used to monitor protein aggregation²⁵. It measures the diffusion rates of particles in solution, which, because the diffusion rate depends on a particle's size and shape, gives their hydrodynamic radius/diameter. Since the size of the DAHPS(Y) dimer is known, if its experimental hydrodynamic radius is significantly larger than the dimer, then the protein is aggregated^{23,24}.

The random Brownian motion of a particle with hydrodynamic radius R_h in solution is described by the Stokes-Einstein equation,

$$D_\tau = \frac{k_B T}{6\pi\eta R_h}$$

where D_τ is the diffusion coefficient (m^2/s), k_B is Boltzmann's constant, T is temperature, η is viscosity, and R_h is the hydrodynamic radius²⁷. Thus, measuring a particle's diffusion coefficient gives its R_h value²⁸. Particles' D_τ values are measured by the DLS instrument by passing a polarized He-Ne laser beam through a sample. The light is scattered upon collision with the particles in solution, with each photon scattered at an angle θ . The scattered light is

collected through another lens and detected by a photon detector, which generates an interference, or speckle, pattern²⁹ (Figure 9; Figure 10). The rate of decay of the pattern is obtained from a time correlation function. This gives the distribution of D_τ values of particles in a solution, and therefore their R_h values. The DLS instrument is capable of measuring rates over the range of μs to several seconds, which is useful because the average protein diffusion time is between 1 and 100 milliseconds²⁸.

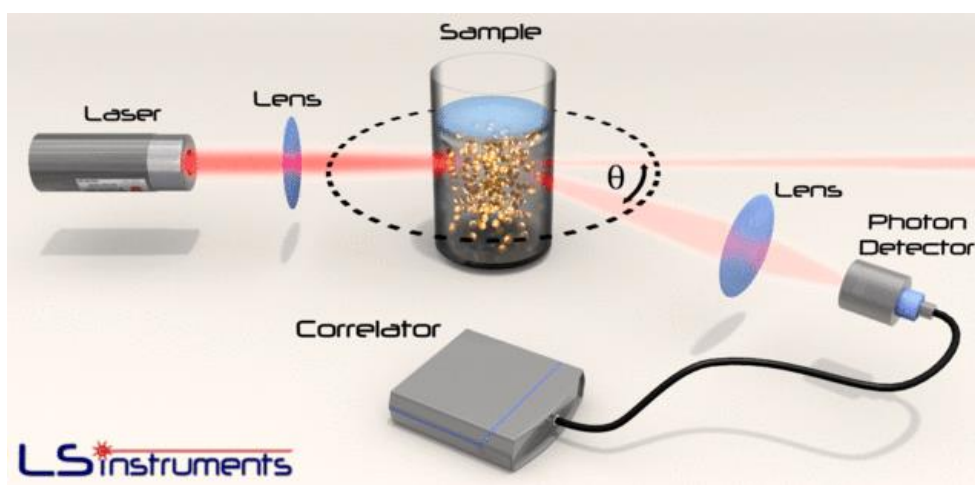


Figure 9: Schematic of a DLS spectrometer.

(Image from <https://lsinstruments.ch/en/technology/dynamic-light-scattering-dls.>)

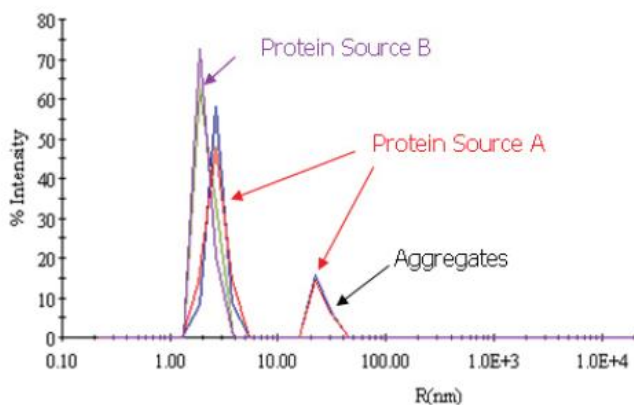


Figure 10: Example DLS spectra.

The hydrodynamic radii (R) of example proteins are shown. (Figure from <http://ipimediaworld.com/wp-content/uploads/2012/05/Pages-from-IPI-Volume-2-Issue-1-3.pdf>.)

A soluble 80 kDa protein will typically have $R_h \approx 4$ nm. Larger particles would indicate protein aggregation. An aggregated protein may show two peaks, one corresponding to the native form, and the other to the aggregated form²⁸.

1.3.2. Methods to Prevent Aggregation

Protein aggregates, i.e., clusters of unfolded or misfolded protein molecules, can often be stabilized using non-covalent interactions, such as hydrogen bonding, dipole-dipole interactions and hydrophobic attractions. Protein aggregation is a large concern in biopharmaceuticals manufacturing, as it leads to activity loss and degradation, and can happen at any stage from production to administration³⁰. Thus, it is necessary to understand ways to prevent aggregation from occurring, both at the production and purification stages.

Magnesium Chloride ($MgCl_2$)

At low concentrations, some salts, such as $MgCl_2$, can stabilize proteins through nonspecific electrostatic interactions³¹. However, at high concentrations, they can either stabilize or destabilize the protein by binding to the water molecules surrounding the protein³¹. Beyond $MgCl_2$'s general effects on protein stability, DAHPS requires a divalent metal cation for activity³². Mg^{2+} does not activate DAHPS appreciably, but given its broad metal-ion specificity, there is reason to expect that it will be able to bind in DAHPS's metal binding site and stabilize the protein.

Tris(2-carboxyethyl)phosphine (TCEP)

TCEP is an antioxidant that is capable of reducing disulfide bonds to cysteine residues^{33,34}. Adding 5 mM TCEP reduced aggregation of *Penicillium chrysogenum* acyl coenzyme A: isopenicillin N acyltransferase, as detected by DLS³³, from ~50% of the protein to undetectable.

Arginine and Glutamic Acid

In some cases, the combination of 50 mM each of glutamic acid and arginine has been shown to increase protein solubility and stability³⁵. At high concentrations, arginine has been shown to improve the ability of recombinant proteins in *E. coli*, allowing refolding within inclusion bodies by suppressing the aggregation of folding intermediates during thermal unfolding or refolding. There are two possible mechanisms that have been studied to explain how this works. These include the ability of additives, such as arginine, to interact with the amino acid side-chains in the peptide sequence, and the water molecules surrounding the protein to help stabilize them³⁶.

1.4. Inhibitor Design

1.4.1. Fragment-Based Inhibitor Design

Fragment-based inhibitor design involves “evolving” high affinity inhibitors for the target of interest from smaller, low affinity fragments^{37,38}. Commonly during drug discovery, “Lipinski’s rules” are used as a guideline. However, antibiotics have been considered exceptions to these rules, as they commonly have higher molecular weights and polarity³⁹.

There are three stages that lead to fragment-based design. First, a target is selected, for which there is a fragment library designed. These fragments are then screened for binding using activity assays or biophysical techniques, such as 1D/2D NMR, X-ray crystallography or mass spectrometry. Finally, the fragment is elaborated using structural information, *in silico* design and information on bioaffinity^{37,38} (Figure 11).

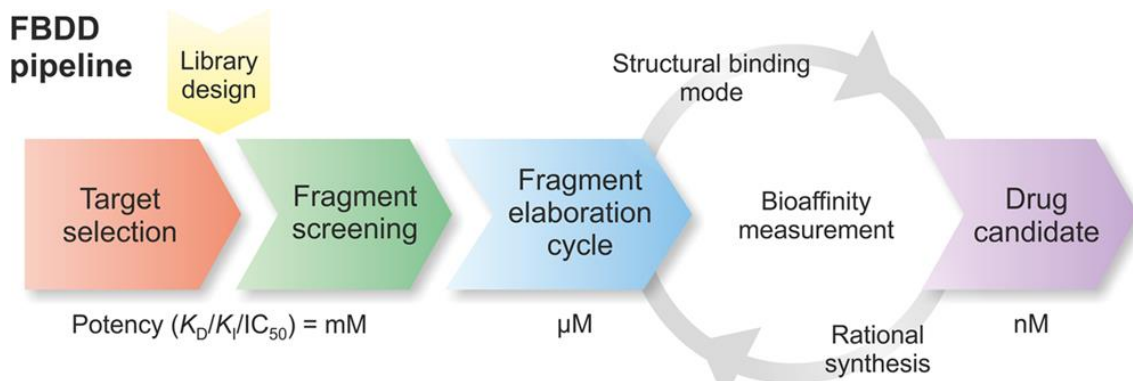


Figure 11: Workflow of fragment-based drug discovery (FBDD).

FBDD begins with the selection of a target, leading to screening, elaboration and finally optimizing the fragment to obtain a potent inhibitor³⁷.

1.4.2. Inhibitor Design with DAHP Oxime and DAHP Hydrazone

Previously in our lab, there have been two archetypal DAHPS inhibitors. DAHP oxime has $K_i = 1.5\mu\text{M}$ and a residence time of 83 mins⁴ (Figure 12). Its fragment analogue is the combination of pyruvate oxime and glycerol 3-phosphate (Gro3P). Neither fragment on its own is an inhibitor, but the combination gives DAHPS inhibition⁵. The combination of the two fragments is the structural equivalent of DAHP oxime with the C4-O4 bond removed. Using this inhibitor-in-pieces approach makes it possible to rapidly test small fragments in the oxime location without the challenge of synthesizing the full-sized DAHP analogue.

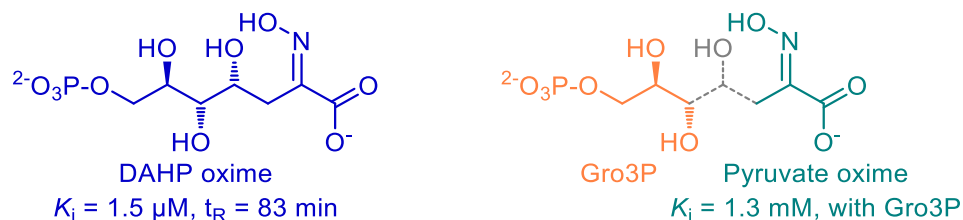


Figure 12: DAHP oxime and pyruvate oxime.

Pyruvate oxime is unable to inhibit DAHPS on its own but has a $K_i = 1.3 \text{ mM}$ in the presence Gro3P.

Oxime-based inhibitors have been shown to inhibit all three major members of the NeuB superfamily of α -carboxyketose synthases – DAHPS^{4,5}, KDO8PS⁴⁰, and NeuB⁴¹, suggesting that oxime-related inhibitors are likely to be universal inhibitors of this class of enzyme. Substituting the OH of the oxime for NH_2 in DAHP hydrazone increased inhibitor binding 150-fold, with the K_i value decreasing to 10 nM ⁴². This increased affinity can likely be attributed, at least in part, to an additional water molecule, HOH2, observed in the crystal structure (Figure 14). HOH2 can form a bridge between the hydrazone NH_2 group and the Arg234 sidechain. One possible means to further increase the inhibitor's binding would be to introduce an oxygen atom into its structure in the same location as HOH2.

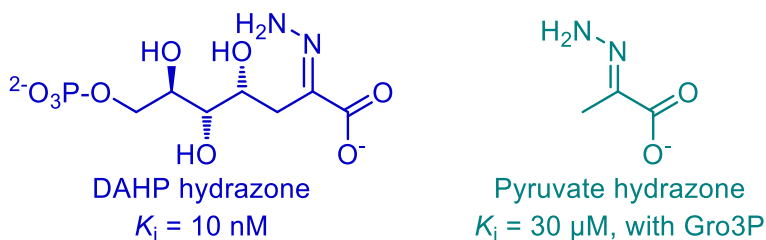


Figure 13: DAHP Hydrazone to Pyruvate Hydrazone (fragment).

Pyruvate hydrazone has a $K_i = 30 \mu\text{M}$ in the presence of Gro3P.

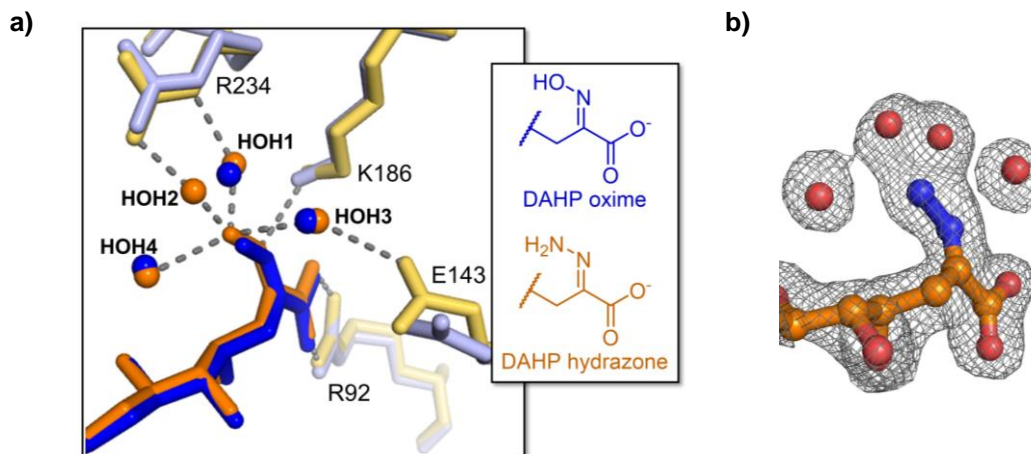


Figure 14: DAHPS(F)•DAHP hydrazone structure.

(a) Water coordination of DAHP hydrazone in the DAHPS(F) active site. HOH1, 3, 4 are located in similar positions with both DAHP hydrazone (orange) and DAHP oxime (blue). HOH1 and HOH3 occupy the same positions as the non-bridging phosphate oxygen atoms of PEP, and HOH4 is present in DAHPS(F)•PEP•Mn²⁺.⁴³ HOH2 is an additional water not seen in other structures that bridges from the hydrazone -NH₂ to the R234 sidechain. (b) Electron density around the hydrazone functional group (2Fo – Fc map, contoured at 1.0 σ). (Crystal structure solved by M. Heimhalt. Figure prepared by Dr. Berti.)

The pyruvate hydrazone derived from the DAHP hydrazone is modified by adding a *N*-formyl group to provide a water mimic (Figure 15). This is predicted to allow for better binding to the inhibitor site.

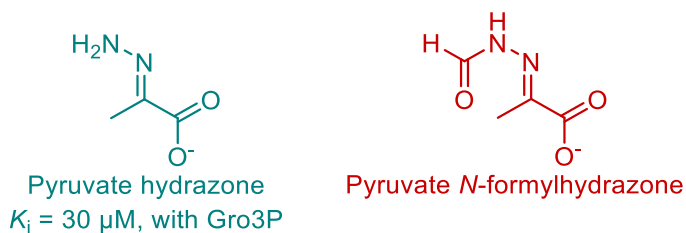


Figure 15: Pyruvate hydrazone to Pyruvate-*N*-formylhydrazone

(PFH; First synthesized by Vanessa Di Cecco).

Previous work has shown that there are multiple benefits to displacing water as a means of increasing target-inhibitor binding efficacy. It has been observed that if an inhibitor is able to displace bound water molecules, there needs to be a replacement for the water, which is the *N*-formyl group in the case of the PFH, to help stabilize the protein⁴⁴.

Reducing the oxime group of pyruvate oxime to an *N*-hydroxylamine functional group gave *N*-hydroxyalanine, which is currently being tested by our lab (Figure 16).

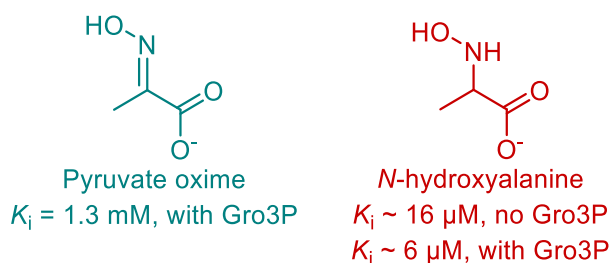


Figure 16: Pyruvate oxime to *N*-hydroxyalanine

(NHA; Synthesized by James Anupol).

With the reduction of the imine group, C2 is modified from sp^2 to sp^3 hybridization to provide a tetrahedral center, which may allow it to bind to the active site more tightly. With tighter binding, it would allow for the inhibitor to be more potent than the parent molecule. Unlike pyruvate oxime, it exhibited inhibition in the presence and absence of Gro3P. This would imply that when the inhibitor fragment will be extended to the full-length DAHP version, it will be highly potent.

1.4.3. Summary of Inhibitor Design

Using fragment-based inhibitor design allows for a better understanding of the chemistry of the individual fragments, which would allow for better prediction of the effects of the full-sized DAHP inhibitor.

2. Materials and Methods

2.1. Materials

2.1.1. General

E. coli DAHPS(F) and DAHPS(Y) used for kinetic experiments were expressed and purified by Rebecca Turner, Jessica Mo and me. TEV protease used to cleave the His-tag on the DAHPS(Y) was expressed and purified by Victoria Brown, Jessica Mo and me. The E4P used for the MG/AM assays were synthesized by Alvin Niu and me. All of the reagents used for the MG/AM, with the exception of MnCl_2 and the enzyme were treated with Chelex 100 to remove metal ions. All additional materials were purchased from Sigma-Aldrich or BioShop, unless otherwise stated.

2.2. Protein production, purification and characterization

2.2.1. Production of Electrocompetent Cells

A 100 μL aliquot of *E. coli* BL21(DE3) was added to 50 mL lysogeny broth (LB) without antibiotics. It was incubated for 16-18 h at 37°C in a shaking incubator at 200 rpm, then transferred to a 1 L of LB, incubated with shaking at 37°C until the optical density (OD_{600}) was 0.5 – 0.6. The cells were centrifuged at $5000 \times g$ for 20 min at 4°C, then resuspended in 250 mL of sterile water and centrifuged again, then resuspended in 200 mL of sterile 10% glycerol and centrifuged again. The pellet was resuspended in an equal volume of 10% glycerol, flash-frozen on a dry ice / ethanol bath, and stored at -80°C.

2.2.2. Production of Chemically Competent Cells

Chemically competent cells were produced following the same procedure, up to first centrifugation step. After centrifugation, the pellet was resuspended in 10 mL of chilled sterile 0.1 M CaCl₂ and incubated on ice for 20 min, followed by centrifugation again. The pellet was resuspended in 5 mL of 0.1 M CaCl₂ and 15% glycerol. The cells were flash frozen in 200 µL aliquots on a dry ice / ethanol bath, then stored at -80°C.

2.2.3. Plasmid Transformation using Electroporation

A 200µL aliquot of electrocompetent cells was thawed on ice, along with the plasmid, and two electroporator cuvettes. The cells aliquoted into the cuvettes, and 100 ng of plasmid was added to one cuvette while nothing was added to the control. The cells were pulsed in the electroporator at 2500V, then immediately transferred to 800 µL SOC medium at 37°C, incubated with mixing for ~ 60 min, then plated on an LB agar plate containing the appropriate selection antibiotic (100 µg/mL of ampicillin or 30 µg/mL of chloramphenicol), then incubated overnight at 37°C. The following day, one colony was selected to start the expression culture.

2.2.4. Plasmid Transformation using Heat-Shock

The competent cells were treated with 100 ng of plasmid and put on ice for 10 min. The cells were then heated at 42°C for 2 min and then placed back on ice for 2 min. SOC media (800 µL) was added and the SOC-cell mixture was incubated at 37°C for 45-60 min. The cells were plated and left overnight at 37°C.

2.2.5. DAHPS(Y) Expression and Purification

DAHPS(Y) was expressed in LB medium. Using electroporation, the bacterial cells were transformed with the DAHPS (Y) plasmid and plated on LB agar containing 100 µg/mL ampicillin, then incubated at 37°C overnight. The next morning, one colony was transferred to 50 mL of LB medium containing 100 µg/mL ampicillin. The flask was incubated at 37°C overnight with mixing at 200 rpm. The next morning, the culture was transferred to 1 L of LB medium with 100 µg/mL ampicillin and incubated at 37 °C at 200 rpm in a shaking incubator. When OD₆₀₀ reached 0.5 - 0.6, 300 µM isopropyl β-thiogalactoside (IPTG) was added to induce protein expression, and the culture was incubated for 4 h at 37°C with mixing at 200 rpm. The culture was then centrifuged at 5000 × g for 20 min at 4°C and frozen at -80°C until purification. The cells were resuspended in 5 mL/g of cells of Buffer A (50 mM Tris-Cl, pH 8.0, 150 mM KCl, 25 mM imidazole, 10% glycerol) and lysed in a Constant Systems cell disruptor at 40,000 psi at 4°C. Protease inhibitor cocktail (10 µL/mL of lysate) was added. The lysate was centrifuged at 8000 × g for 30 min at 4°C. The supernatant was filtered through a 0.45 µm filter. It was then applied to a 1mL Ni²⁺-charged HiTrap Chelating-Sepharose column, which was washed with 20 column volumes of Buffer A at 1 mL/min, followed by 10 column volumes of 10% Buffer B (50 mM Tris-Cl, pH 8, 150 mM KCl, 500 mM imidazole, 10% glycerol). The protein was eluted with 10 column volumes each of 80% Buffer B and 100% Buffer B. Each of these fractions were collected and absorbance readings at 280 nm (A₂₈₀) were taken. The concentration of DAHPS(Y) was determined from the A₂₈₀ and $\epsilon_{280} = 18,480 \text{ M}^{-1} \text{ cm}^{-1}$ (E. Curiel-Tejeda, personal communication).

The His₆-tag was removed using tobacco etch virus (TEV) protease⁴⁵. It was added in a TEV protease:DAHPS(Y) molar ratio of 1:4 in the 80% Buffer B fraction and incubated overnight at 4 °C. The cleaved protein was dialyzed overnight at 4 °C against 20 mM Tris-Cl, pH 7.5.

The dialysate was then loaded onto a 1 mL Ni²⁺-charged HiTrap Chelating-Sepharose and the now non-His₆-tagged DAHPS(Y) was eluted in Buffer A. The column was then washed using 80% Buffer B to elute the His₆-TEV protease, uncleaved DAHPS(Y), and the cleaved His₆-tag. Eluted DAHPS(Y) was dialyzed against Dialysis Buffer 1 (50 mM Tris-Cl, pH 8, 150 mM KCl, 1 mM EDTA, 10% glycerol) at 4°C overnight, then dialyzed against Dialysis Buffer 2 (50 mM Tris-Cl, pH 8, 150 mM KCl, 10% glycerol) at 4°C for 4 h. Purified DAHPS(Y) was flash frozen in a dry ice / ethanol bath and stored at -80 °C in 200 µL aliquots. Its purity was assessed by 13% SDS/PAGE electrophoresis.

2.2.6. DAHPS(F) Expression and Purification

E. coli BL21(DE3) cells were transformed with the DAHPS(F) plasmid, as described previously⁴. DAHPS(F) was expressed and purified using the same procedure as DAHPS(Y), up to the end of the first Chelating-Sepharose purification step, except the antibiotic was 30 µg/mL of chloramphenicol. At that point, the purified protein was dialyzed in Dialysis Buffer 1 overnight, then Dialysis Buffer 2 for 4 h. The protein concentration was determined from the A₂₈₀ using $\epsilon_{280} = 31,450 \text{ M}^{-1} \text{ cm}^{-1}$ before being flash frozen on a dry ice /ethanol bath and stored at -80°C⁴.

2.2.7. TEV Protease Expression and Purification

E. coli BL21(DE3) cells were transformed with the TEV protease plasmid, as described previously⁴. TEV protease was expressed and purified using the same procedure as DAHPS(F),

except ampicillin (100 $\mu\text{g}/\text{mL}$) was used as the antibiotic. The protein concentration was determined from the A_{280} , using $\epsilon_{280} = 32,410 \text{ M}^{-1} \text{ cm}^{-1}$.⁴⁵

2.2.8. Plasmid Sequencing

The DAHPS(Y) plasmid was isolated for sequencing using a Qiagen MiniPrep kit and sequenced by the Mobix Lab (McMaster University).

2.2.9. Dynamic Light Scattering (DLS)

DLS spectra were collected at 4°C on a Zetasizer Nano ZS DLS spectrometer. 40 μL of 10 μM enzyme in 10mM ammonium acetate was added to the cuvette. The buffer composition was entered into the Zeta software and the refractive index of water was selected as a reference. Each sample was run for approximately 5 min and repeated three times.

2.2.10. Rate assays using Malachite Green/ammonium molybdate (MG/AM) detection

DAHPS reaction rates were measured by detecting the production of inorganic phosphate (P_i) using the Malachite green/ammonium molybdate (MG/AM) colorimetric assay^{4,46}. Rate assays were conducted in 200 μL of Kinetic Buffer (50 mM K-HEPES, pH 7, 100 mM KCl, 100 μM TCEP). Typically, the substrate concentrations were 100 μM MnCl_2 , 500 μM PEP, 50 μM E4P. The reaction was started by adding enzyme last, at concentrations of 20 to 100 nM. The Kinetic Buffer, PEP and E4P solutions were treated with Chelex 100 before use to remove metal ions. Aliquots (20 μL) were transferred to the MG/AM solution in a 96 well plate at varying time points. Sodium citrate (10 μL , 34%) was added after ~75 s to stop colour development, and A_{660} was read when the reaction was complete.

2.2.11. Synthesis and Purification of Erythrose-4-Phosphate (E4P)

DAHPS's second substrate, erythrose-4-phosphate (E4P), was synthesized by oxidizing glucose 6-phosphate (G6P) with lead tetraacetate^{4,47}. Briefly, G6P was dissolved in acetic acid, and aliquots of $\text{Pb}^{4+}(\text{OAc})_4$ were added to oxidize it to E4P. Excess G6P was used to avoid over-oxidization products, like glyceraldehyde 3-phosphate, which is a known DAHPS inhibitor^{15,47}. Starch-iodide indicator paper was used to ensure that the Pb^{4+} in each aliquot had been consumed before another was added. Starch-iodide paper turns blue in the presence of Pb^{4+} , and remains white in its absence⁴⁷. E4P was purified by anion exchange chromatography on Q-Sepharose, with E4P elution detected using the reducing sugar assay (RSA) in which aldehyde functional groups reduce Cu^{2+} to Cu^+ , which then complexes with the chromophore, neocuproine, giving absorbance at 450 nm⁴⁸. Since G6P is also a reducing sugar, G6P and E4P cannot be differentiated using the RSA. Chromatographic fractions were sometimes assayed for activity with DAHPS using the MG/AM assay to detect E4P specifically. The G6P dehydrogenase assay was used to detect G6P specifically⁴⁹. Finally, NH_4^+ ions from the anion exchange step were removed by cation exchange chromatography on Amberlite (H^+) cation exchange resin.

2.2.12. Alkaline Phosphatase (APase) Assay

Alkaline phosphatase (APase) is a non-specific phosphatase that can be used to detect phosphate-containing compounds by releasing P_i , which is then detected with the MG/AM assay. APase (6.4 mg) was dissolved in 1.5 mL of APase Buffer (25 mM Tris-HCl, pH 7.6, 1 mM MgCl_2 , 0.1 mM ZnCl_2 , 50% w/v glycerol). The reaction mix was prepared by adding 10 μL of sample in 190 μL of water. The APase reaction was started by adding 5 μL of enzyme solution to

the 200 μL reaction mixture and taking a 20 μL aliquot every minute. The concentration of Pi produced by the reaction was assayed using the MGAM colorimetric assay.

2.3. Inhibitor Synthesis and Testing

2.3.1. Lactate dehydrogenase (LDH) assay

Inhibitor synthesis reactions were monitored by the loss of pyruvate from the reaction mixture. Pyruvate concentrations were monitored using the lactate dehydrogenase (LDH) reaction in which pyruvate is reduced to lactate, with a concomitant oxidation of NADH to NAD^+ ($\Delta\epsilon_{340} = 6220 \text{ M}^{-1} \text{ cm}^{-1}$)⁵⁰. LDH (5mg/mL) was prepared in 0.05 M Tris-HCl, pH 7.6, 0.12 M KCl, 0.062 M MgSO_4). The reaction mix was prepared by adding 50 μL of 45 mM ADP, 50 μL of 6.6 mM NADH and 25 μL of sample in 1.5mL of buffer. The reaction mixture was placed in a cuvette in the spectrophotometer, and when A_{340} was stable, 5 μL of the LDH solution was added. The reaction was monitored until A_{340} was stable again, and the pyruvate concentration calculated from ΔA_{340} .

2.3.2. Pyruvate-N-Formylhydrazone (PFH) Synthesis

Sodium pyruvate (1 M) was reacted with 1.5M formic acid hydrazide (FAH) in 1mL of water. The reaction was monitored using the LDH assay. PFH was purified by anion exchange chromatography using a 1mL Q-Sepharose column with a gradient of 1.6 to 80 mM ammonium acetate in water for 30 min at a flow rate of 1mL/min. PFH eluted between 10 - 18 min.

2.3.3. Inhibitory Testing of PFH using the MG/AM Assay

DAHPS(F) inhibition by PFH was tested using the MG/AM activity assay. The substrate mix containing 500 μM PEP, 50 μM E4P, and 100 μM MnCl_2 was prepared in reaction buffer (50 mM K-HEPES, pH 7, 100mM KCl, 100 μM TCEP). For inhibition assays in the presence of Gro3P, 3mM Gro3P was added to the substrate mix. This mixture was adjusted to pH 7 and was aliquoted into reaction tubes containing 0 to 20 mM PFH in a total reaction volume of 200 μL . The reaction was catalyzed using 20nM DAHPS(F) and was run for 5 min at each inhibitor concentration.

The inhibition data were fitted to equation 1, which described the previously determined kinetic mechanism for an inhibitor that is competitive with respect to PEP and E4P, and non-competitive with respect to Mn^{2+} ,⁵ using the previously reported Michaelis-Menten kinetic constants:⁴

$$\frac{v_0}{[E]_0} = \frac{\frac{k_{\text{cat}}[\text{Mn}][\text{PEP}][\text{E4P}]}{K_{\text{M,Mn}}K_{\text{M,PEP}}K_{\text{M,E4P}}}}{\left(1 + \frac{[I]}{K_i}\right) \left(1 + \frac{[\text{Mn}]}{K_{\text{M,Mn}}}\right) + \frac{[\text{Mn}][\text{PEP}]}{K_{\text{M,Mn}}K_{\text{M,PEP}}} + \frac{[\text{Mn}][\text{PEP}][\text{E4P}]}{K_{\text{M,Mn}}K_{\text{M,PEP}}K_{\text{M,E4P}}}} \quad (1)$$

The rate versus inhibitor concentration data were fitted to this equation by non-linear regression using the program GraFit (Erithacus Software Limited).

2.3.4. DAHP Synthesis

DAHP was synthesized by reacting 4.2 mM PEP and 4 mM E4P with 400 nM DAHPS(F) and 10 μM MnCl_2 . The reaction took place at room temperature at pH 7 in 50mM K-HEPES, 100mM KCl, and 10 μM TCEP (total reaction volume = 5mL). The reaction was run for 3 h. The

DAHP was purified using the 1mL Q-Sepharose column eluted with a gradient of 0.1 to 0.8M ammonium formate, pH 6.2. The concentration was tested using the APase assay.

2.3.5. Pyruvate Oxime Synthesis

Sodium pyruvate (5 mmol) was mixed with 10 mmol of hydroxylamine hydrate in 5 mL of water, the pH was adjusted of 6.5 using NaOH, and allowed to react for 3 hours at room temperature as described previously⁵. The consumption of pyruvate was monitored using the LDH assay.

3. Results

3.1. Protein Dynamics

3.1.1. Expression and Purification of DAHPS(Y)

DAHPS(Y) was expressed and purified multiple times (Figure 17) but showed no measurable enzymatic activity.



Figure 17: DAHPS(Y) Purification.

Each lane contained 20 pmol of protein. Lanes: 1) molecular weight stands, 2) DAHPS(Y) purified on Ni-Sepharose, 3) TEV-Cleaved DAHPS(Y), 4) - 8) Stages of DAHPS(Y) dialysis. The expected molecular weight of DAHPS(Y) is 41 kDa before TEV-tag cleavage, and 38 kDa after.

To see if it was because of a problem in our purification method, we expressed and purified DAHPS(F) (Figure 18) and showed that it had activity (Figure 19).

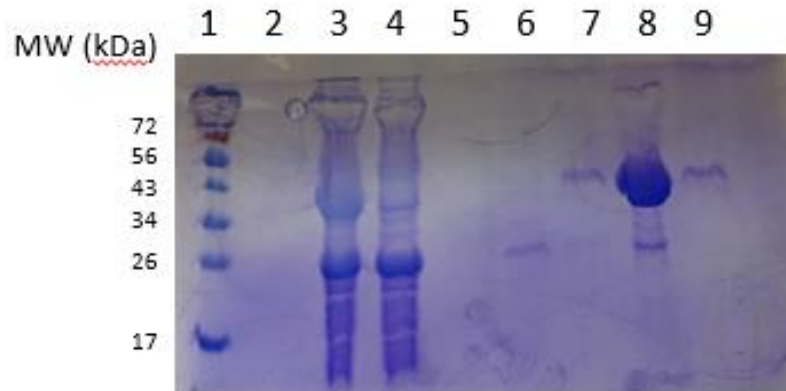


Figure 18: DAHPS(F) Purification.

Lanes: 1) molecular weight stands, 2) Blank, 3) Filtrate, 4) Run Through from Ni-Sepharose, 5) Blank, 6) – 9) DAHPS(F) purified on Ni Column. The expected molecular weight of DAHPS(Y) is 41 kDa.

DAHPS(F) activity was measured using the MG/AM colorimetric assay for inorganic phosphate (P_i), the side product of the DAHPS reaction⁴⁶. No $MnCl_2$ was added, as the enzyme appeared to contain a metal ion, presumably Fe^{2+} after purification on the Ni-Sepharose column (Figure 19). This activity decreased with added EDTA. The fact that active DAHPS(F) could be produced indicated that the expression and purification methods were not the cause of DAHPS(Y)'s inactivity.

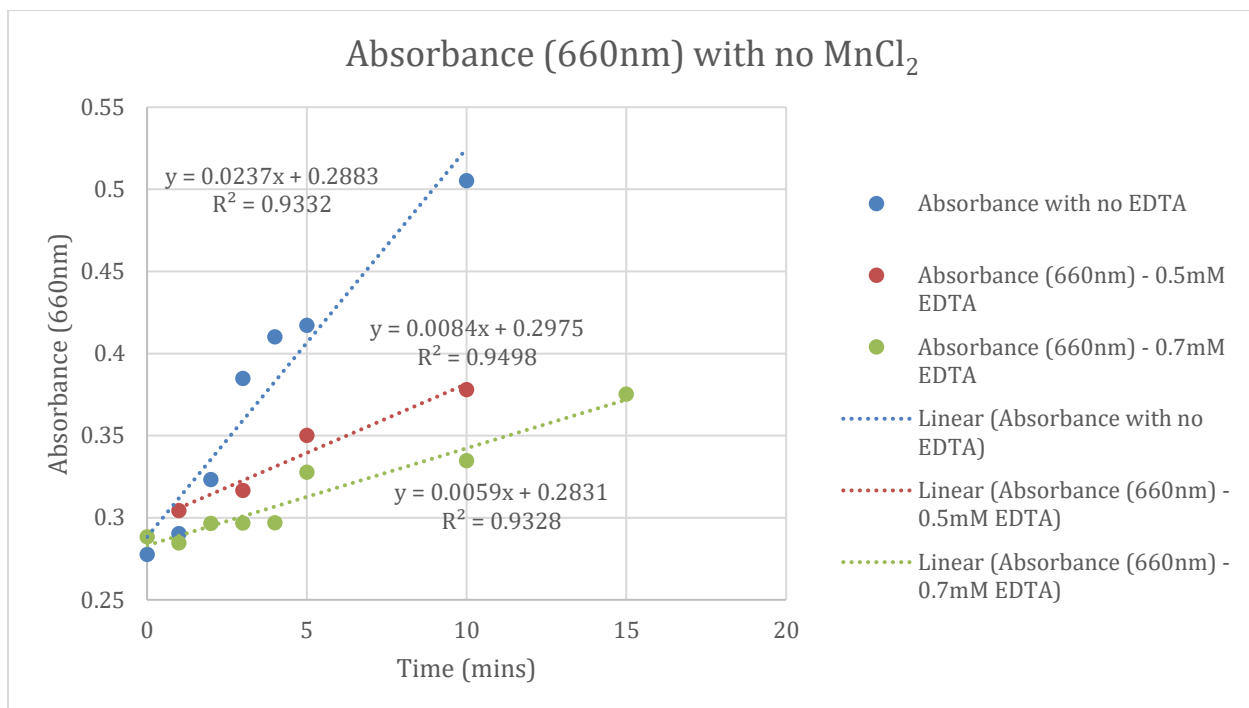


Figure 19: DAHPS(F) activity in the presence of variable EDTA concentrations.

3.1.2. Troubleshooting DAHPS(Y) production

Given DAHPS(Y)'s consistent lack of activity even though it had previously been expressed with good activity in the past, its production was troubleshoot. The plasmid was re-sequenced, and the sequence of the insert was 100% correct. The purified protein was then sent for mass spectrometric analysis at Western University, and the mass was correct to within 1 Da (Figure 34, Appendix 1).

3.1.2.1: Synthesis of Erythrose-4-Phosphate (E4P)

One possible cause of the low DAHPS(Y) activity could have been contaminated E4P. While MnCl₂ and PEP are commercially available, we synthesize our own E4P from glucose 6-phosphate (G6P) via oxidative cleavage with lead tetraacetate (Figure 20)⁴⁷.

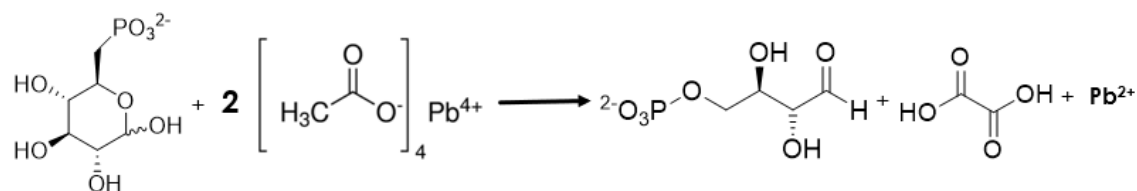


Figure 20: E4P Synthesis

E4P was synthesized by oxidation of glucose 6-phosphate (G6P). (Figure generated by Dr. Berti.)

Yields in recent syntheses had decreased from > 80% to < 10%, which raised the possibility that there was G6P or other contaminants present in the E4P that inhibited DAHPS(Y), but not DAHPS(F), and which had not been present previously. It required numerous attempts to troubleshoot and refine the E4P synthesis.

The initial protocol was meant to react 100% of the G6P with excess lead tetraacetate. However, this was found to not work properly, because it had been discovered that if the G6P is completely reacted, the excess lead is able to further oxidize the E4P to produce glyceraldehyde-3-phosphate (G3P), which is a known inhibitor of DAHP synthase^{15,47}.

Therefore, given the 2:1 Pb^{4+} :G6P stoichiometry in the reaction, 1.7 equivalents of lead tetraacetate was used, 85% of the stoichiometric amount. Starch-iodide indicator paper was used to ensure that all the Pb^{4+} in a given addition had reacted before another aliquot was added. Blue indicated there was still Pb^{4+} present, while white showed it had been consumed⁴⁷.

The next step to refine was purification. Anion exchange chromatography on a Q-Sepharose column to separate G6P from E4P gave good yields. The eluting salt in anion exchange

chromatography was a gradient of ammonium formate. However ammonium ions have been shown previously to lead to E4P degradation⁵¹, so cation exchange was used to exchange NH_4^+ to H^+ . However, there was significant product loss upon cation exchange chromatography on an SP-Sepharose column leading to an overall yield of $\leq 6\%$. To tackle this problem, the SP-Sepharose column was replaced by the Amberlite (H^+) column. This increased the product yield. E4P has a tendency to dimerize when it becomes too concentrated (Figure 21)⁵². Dimerization is reversible, and E4P is a monomer at the concentrations used for enzyme assays.

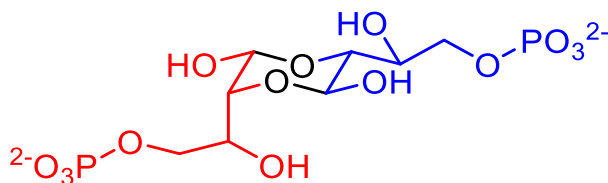


Figure 21: E4P dimer.

E4P at high concentrations can form dimers in solution⁵². (Figure generated by Dr. Berti.).

The fractions were tested using the RSA for the presence and concentration of E4P. As both G6P and E4P are reducing sugars, they reduce Cu^{2+} to Cu^+ , which then complexes with the chromophore, neocuproine, giving absorbance at 450 nm⁴⁸. The G6P concentration was determined using the G6PDH assay.

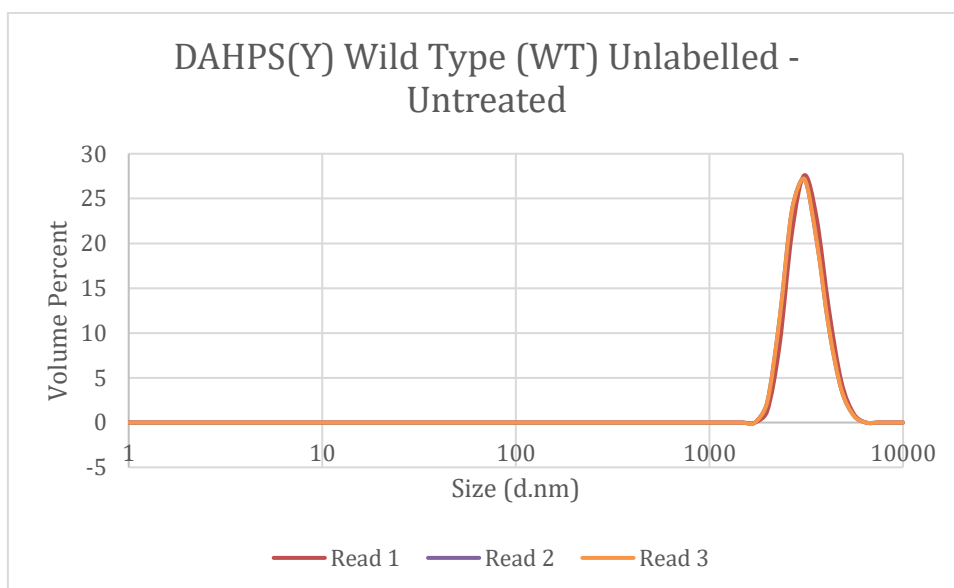
With the new E4P, there was brief activity seen with the DAHPS(Y), but it was not reproducible.

3.1.2.2: Dynamic Light Scattering (DLS)

Thus far, it had been shown that the plasmid sequence for DAHPS(Y) was correct, that the purified protein had the correct molecular weight, and that there was no evidence of problems

with the substrate E4P. The next step was to examine DAHPS(Y)'s solubility and stability using dynamic light scattering (DLS). When unlabeled wildtype (WT) DAHPS(Y) was tested after purification, the hydrodynamic radius of the particles was 1000 to 10,000 nm, compared with the expected value of ≈ 4 nm (Figure 22a). This indicated significant protein aggregation and explained its lack of activity. Although there was aggregation present in FTrp-labelled DAHPS(Y), it was less than for the unlabeled protein (Figure 22b). It was noteworthy that the DLS spectrum of FTrp-labelled DAHPS(Y) changed over the course of three sequential spectra, indicating that aggregation was occurring in the cuvette during the experiment.

a)



b)

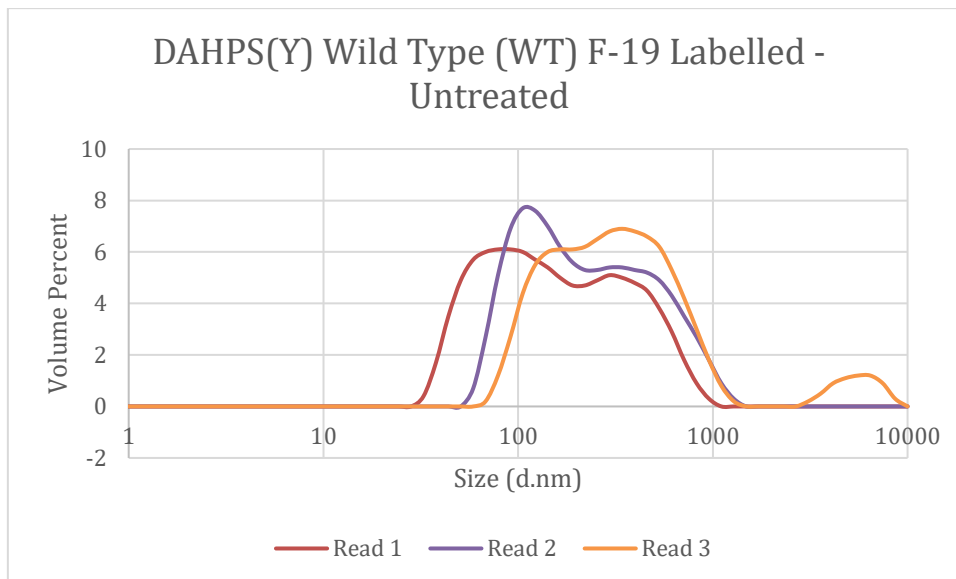


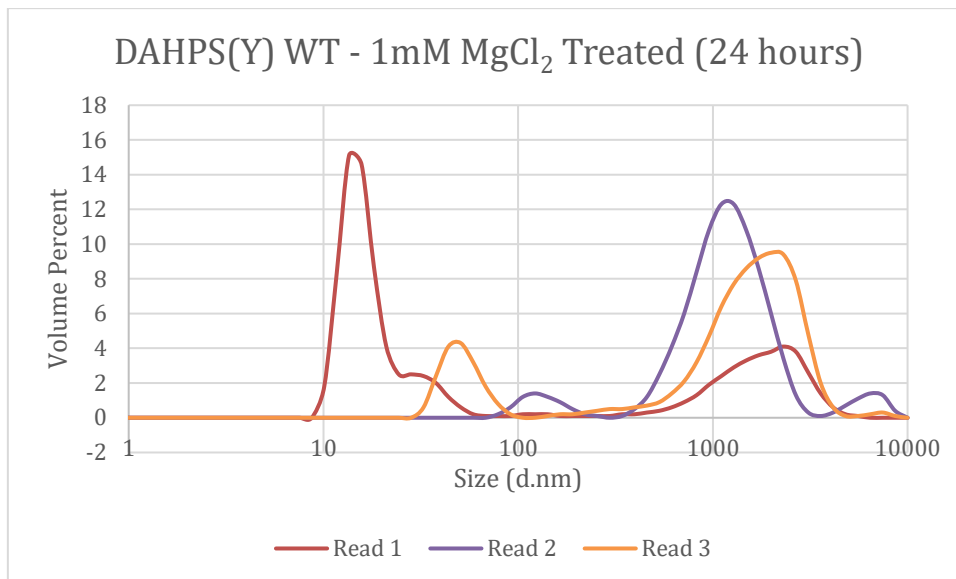
Figure 22: DLS on untreated DAHPS(Y).

a) Unlabelled WT DAHPS(Y) b) FTrp-labelled WT DAHPS(Y).

Based on these results, various treatments were tried to reduce protein aggregation.

Adding 1 mM MgCl_2 for 24 h appeared to decrease the amount of aggregation of both unlabeled DAHPS(Y) and FTrp-labelled DAHPS(Y) (Figure 23). At low concentrations, salts like MgCl_2 , can help to stabilize the proteins through nonspecific electrostatic forces and thereby improve protein solubility³¹. Based on this, it was hoped that adding MgCl_2 would stabilize DAHPS(Y) and reduce aggregation. Again, the extent of aggregation increased through three sequential spectra, indicating that the protein was aggregating during the experiment.

a)



b)

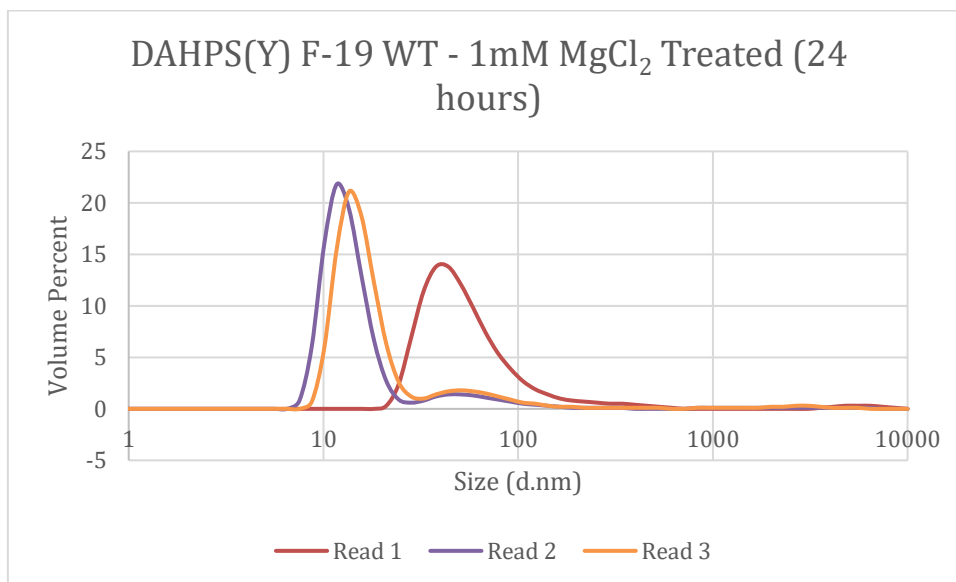


Figure 23: DLS on DAHPS(Y) treated with 1mM MgCl₂.

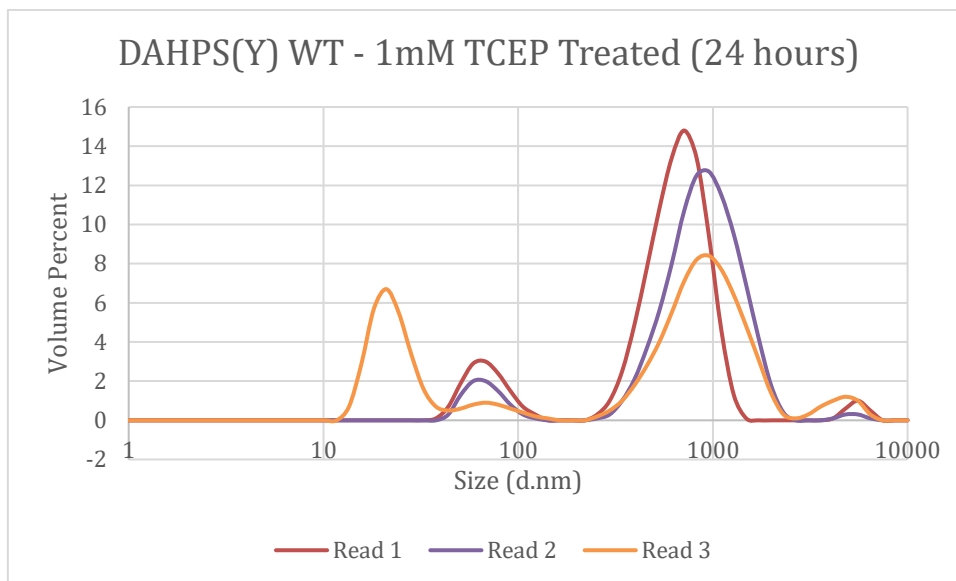
WT DAHPS(Y) treated for 24 h with 1 mM MgCl₂: a) Unlabelled, b) FTrp-labelled.

TCEP is an antioxidant capable of reducing disulfide bonds to Cys residues. Adding 1mM TCEP to the protein samples for 24 h caused a modest reduction in the hydrodynamic diameter of unlabeled DAHPS(Y) (Figure 24a). A large effect was not necessarily expected since

the protein was already badly aggregated, but it did show that TCEP could have some effect.

There was a larger effect with FTrp-labelled DAHPS(Y) consistent with the fact that it was less aggregated to begin with (Figure 24b).

a)



b)

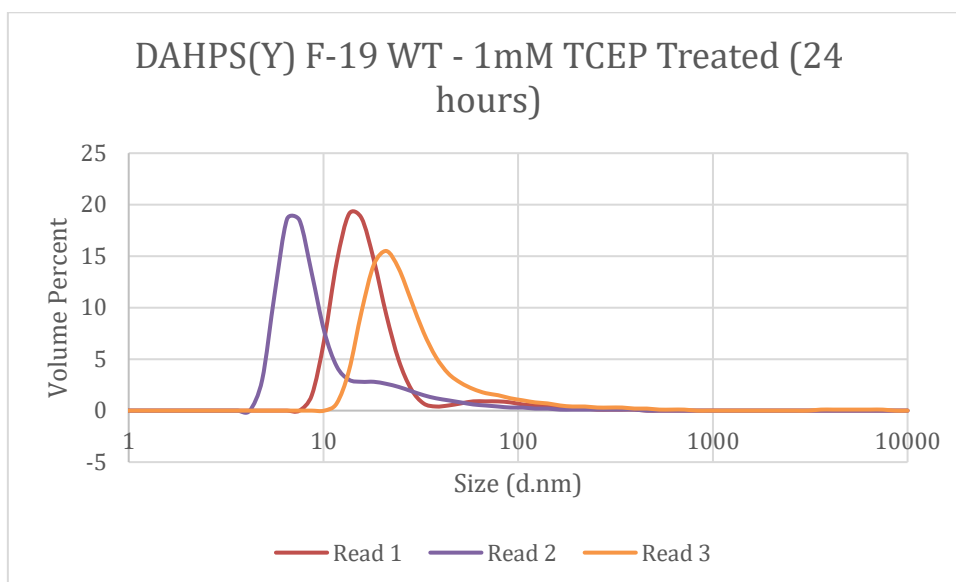
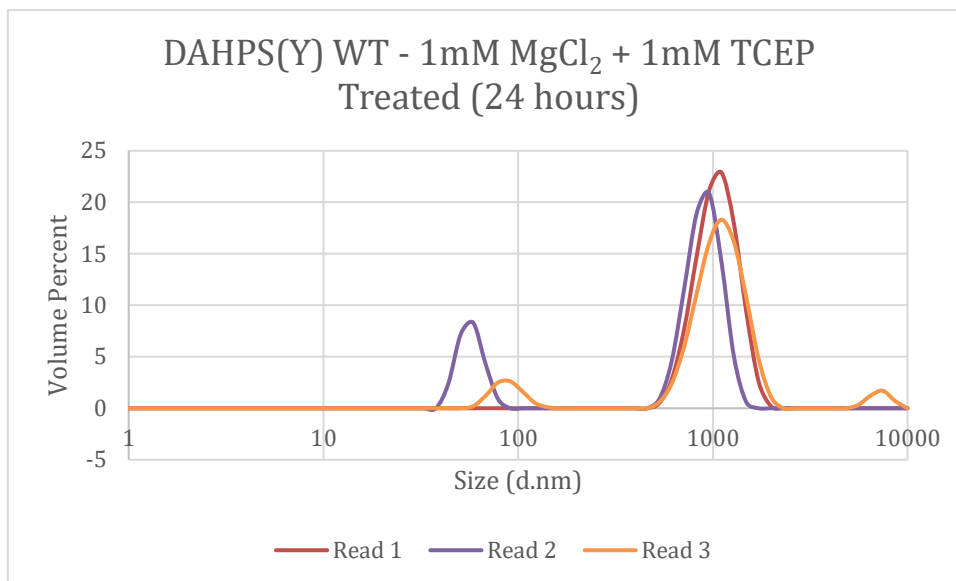


Figure 24: DLS on DAHPS(Y) treated with 1mM TCEP.

WT DAHPS(Y) treated for 24 h with 1 mM TCEP: a) Unlabelled, b) FTrp-labelled.

Unexpectedly, given the effects of MgCl_2 and TCEP individually, the combination of MgCl_2 and TCEP together was not better than either treatment individually (Figure 25). It is unclear why.

a)



b)

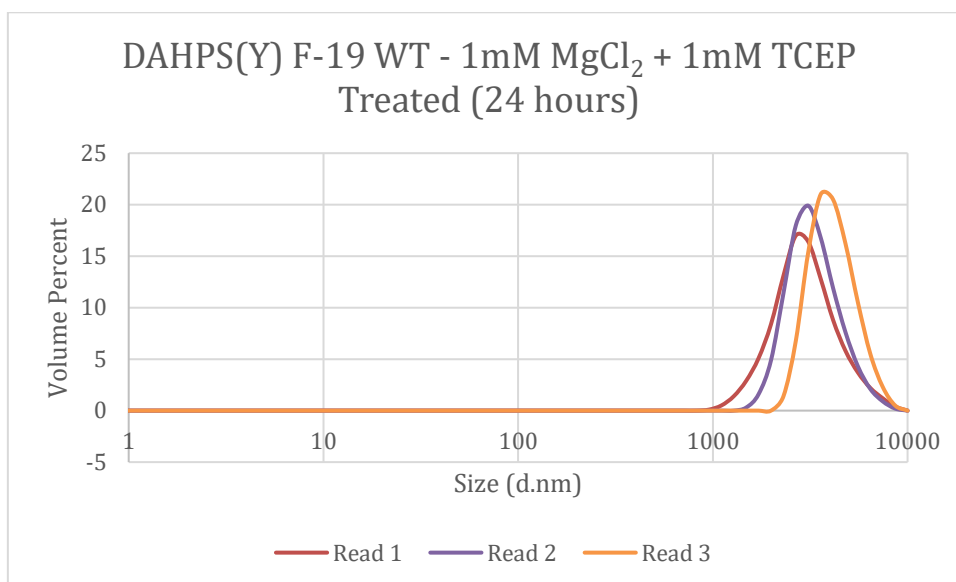


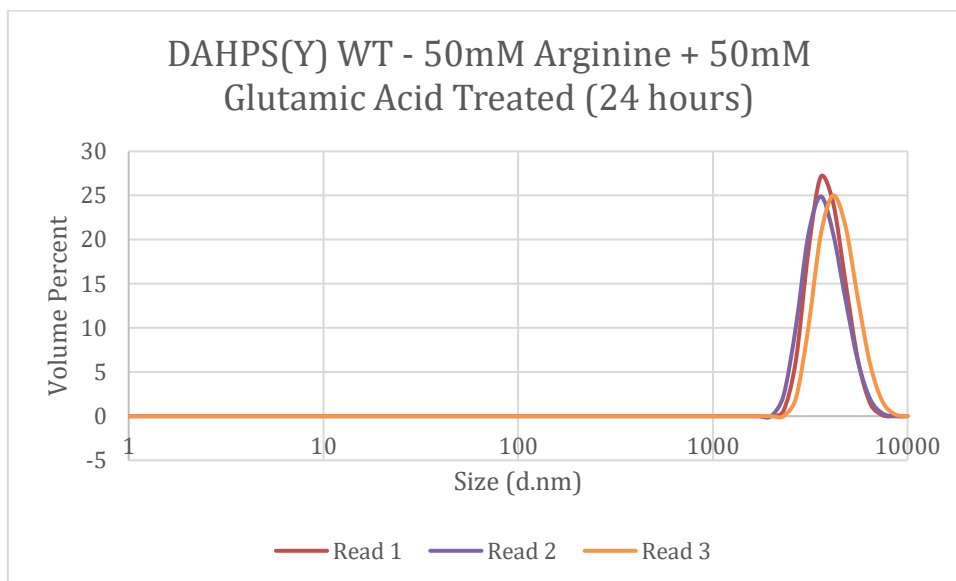
Figure 25: DLS on DAHPS(Y) treated with 1mM MgCl_2 and 1mM TCEP.

WT DAHPS(Y) treated for 24 h with 1 mM MgCl_2 + 1 mM TCEP: a) Unlabelled, b) FTrp-labelled.

Besides extending the time of treatment, Naresh Balachandran, a former PhD student in our lab, added 1mM TCEP during the TEV-tag cleavage and first dialysis step, but added 0.5mM TCEP and 1mM MgCl₂ in the final dialysis step⁵¹, so perhaps lowering the ratio of TCEP to MgCl₂ may work.

In some cases, the combination of 50 mM each of glutamic acid and arginine have been shown to increase protein solubility and stability³⁵. These were tried with DAHPS(Y), but there was essentially no effect on the apparent amounts of aggregation (Figure 26). However, the DLS instrument gave error messages with both samples that the amount of aggregation was too large to measure accurately. Therefore, Glu + Arg did not help with DAHPS(Y) aggregation.

a)



b)

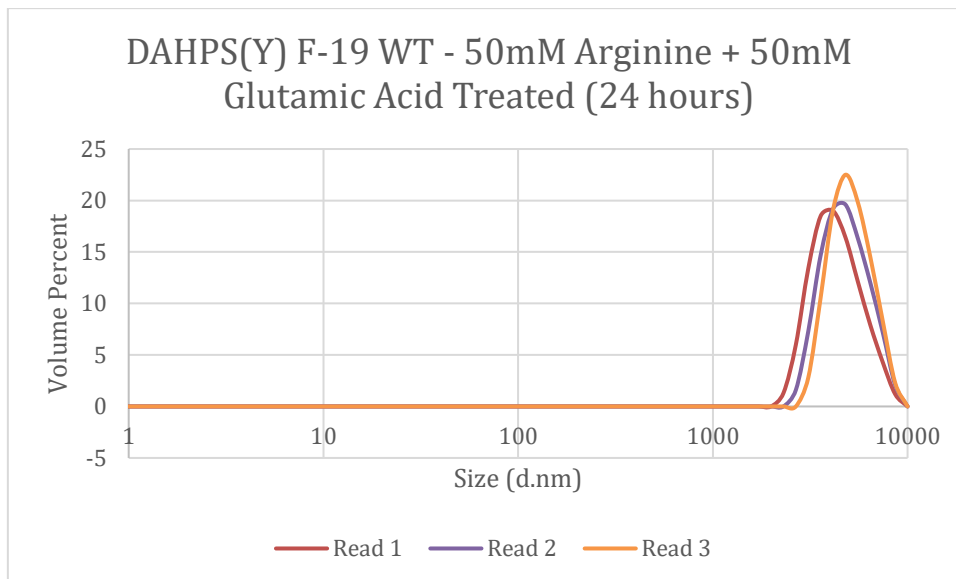
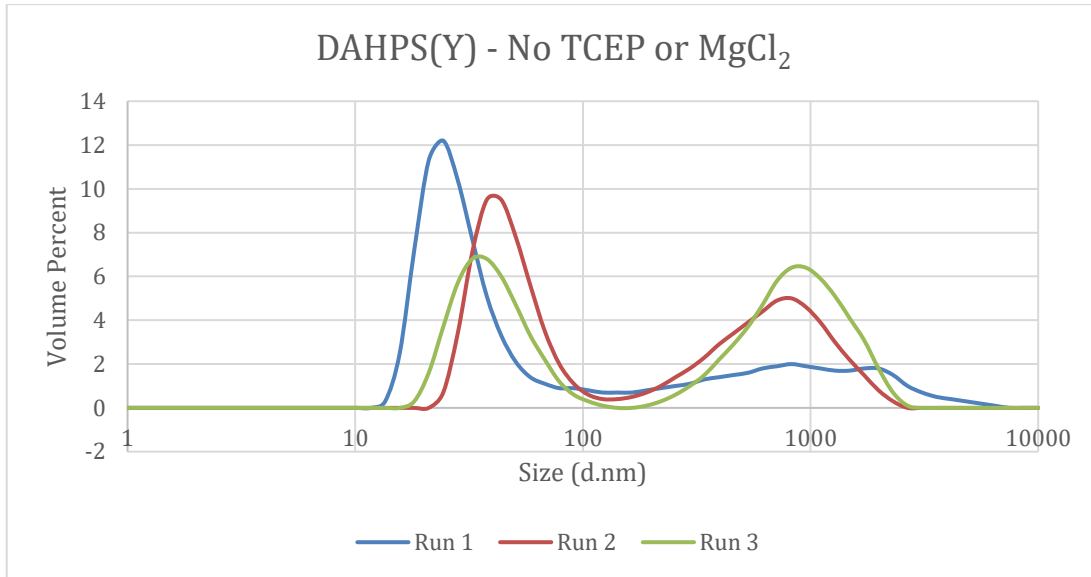


Figure 26: DLS on DAHPS(Y) treated with 50mM Arginine + 50mM Glutamic Acid.

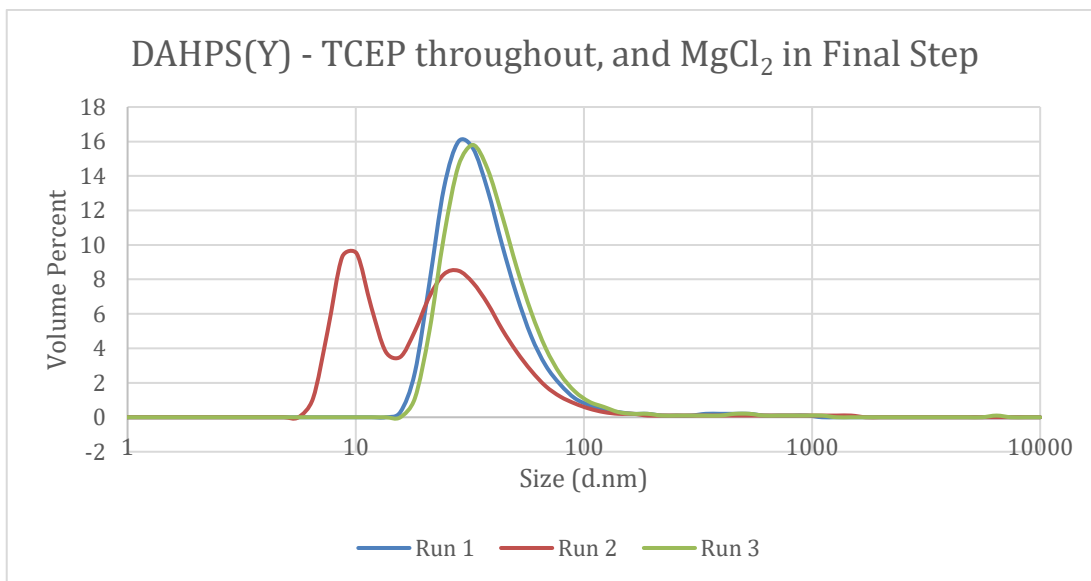
WT DAHPS(Y) treated for 24 h with 50 mM arginine + 50 mM glutamic acid: a) Unlabelled, b) FTrp-labelled.

Since $MgCl_2$ and TCEP appeared to have some effect on protein aggregation in already purified protein, different purification conditions were tried that added them as early as possible in the process. DAHPS(Y) was purified using three protocols: (1) Unchanged, as described in the Materials and Methods section, which did not contain $MgCl_2$, nor TCEP past the TEV protease cleavage step, (2) As above, but with 1 mM TCEP throughout, and $MgCl_2$ in the final dialysis step, (3) As above, but with TCEP and $MgCl_2$ added in each step. However, there was still significant aggregation in the purified protein, and no activity (Figure 27).

a)



b)



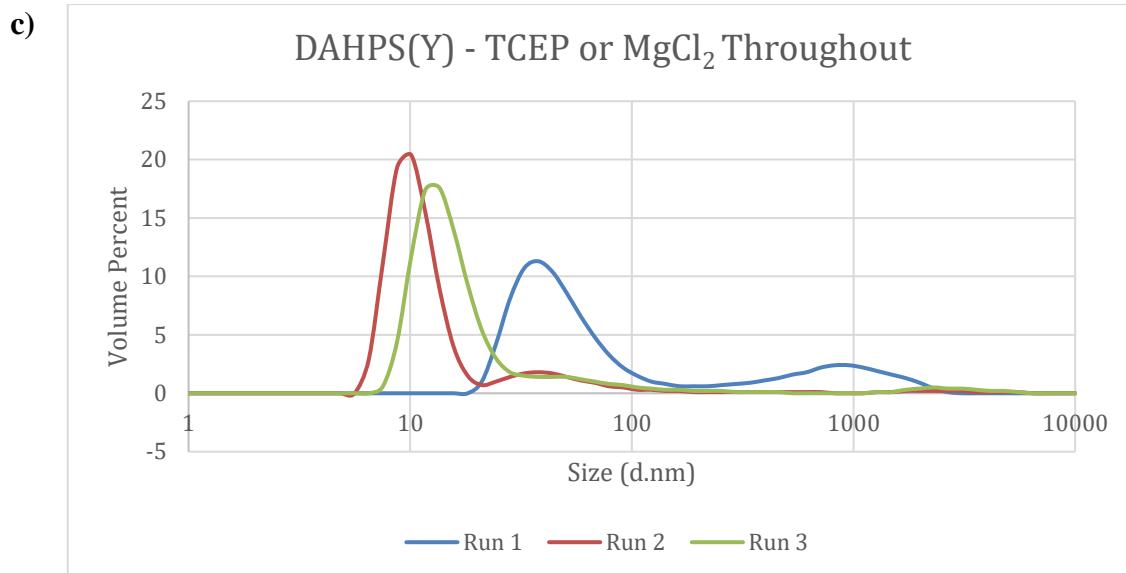


Figure 27: DLS on different purification methods.

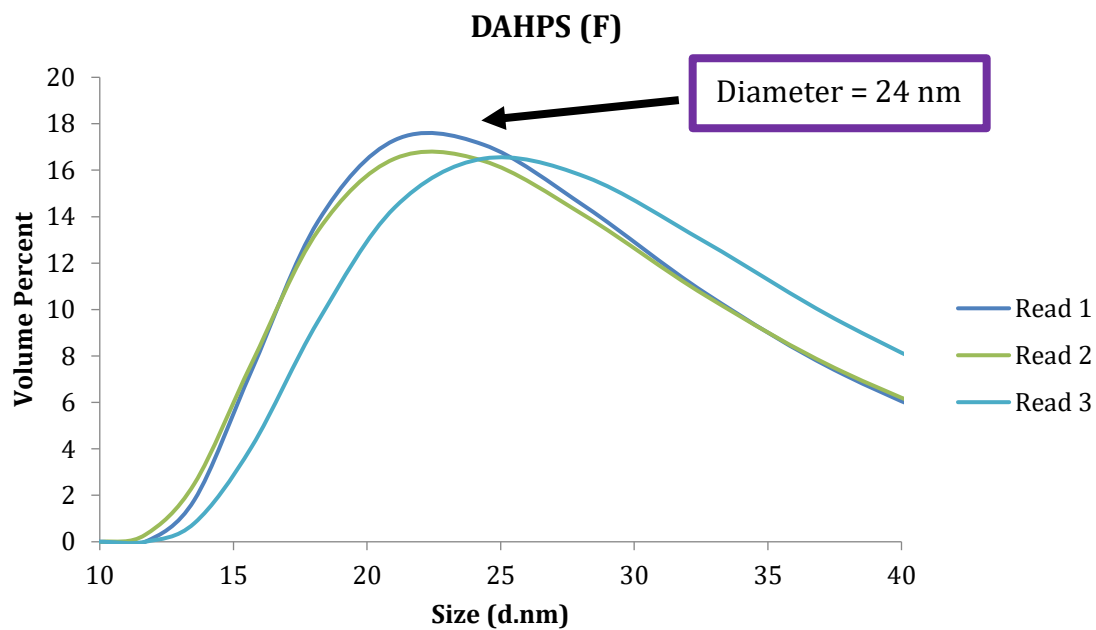
a) Treated with no TCEP or $MgCl_2$, b) Treated with 1mM TCEP throughout and $MgCl_2$ in the final step, c) Treated with TCEP or $MgCl_2$ throughout.

One potential shortcoming of the procedures used to date was that DAHP(Y) activity was only assayed at the end of the purification protocol. Switching to assaying for activity as soon as possible, namely immediately after elution from the Ni-Sepharose column, showed that the protein was not active even at that early stage. Therefore, the protein expression conditions were examined.

Different expression conditions were tested for their ability to produce active enzyme. In each case, the goal was to slow protein production and give the nascent protein time to fold during translation. These techniques have been shown previously to improve the expression of active proteins^{53,54}. (1) The expression temperature was reduced from 37°C to 18°C, with continued induction of protein expression with IPTG. (2) Protein expression at 37 °C overnight in the absence of IPTG. (3) Protein expression at 18°C without IPTG. Only the last conditions produced active

enzyme, with $v_0/[E]_0 = 0.63\text{s}^{-1}$. This was much less than the 10 s^{-1} observed previously (N. Balachandran, personal communication), and was not reproducible. DLS on this purified DAHPS(Y) showed slightly less aggregation and was approximately half of the diameter of DAHPS(F) (Figure 28).

a)



b)

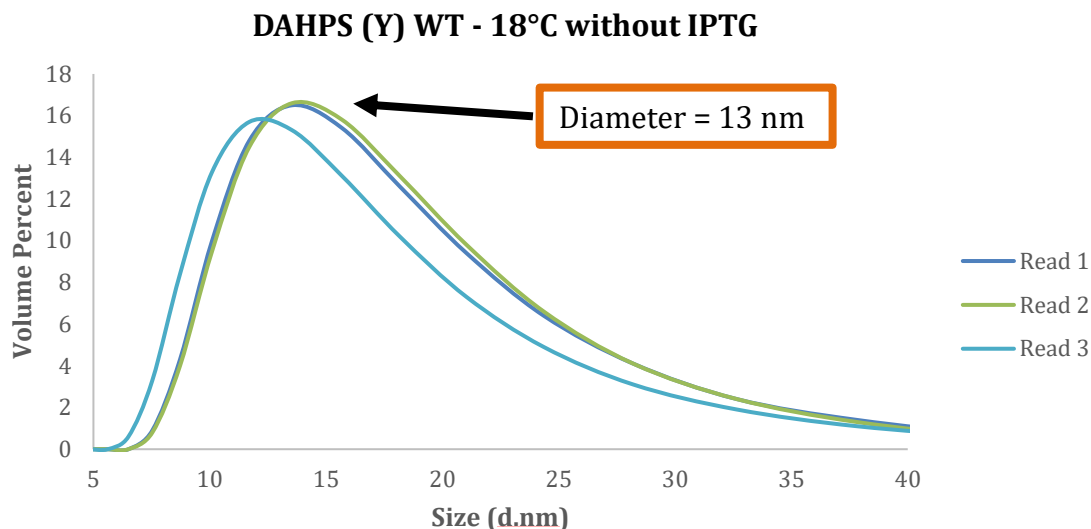


Figure 28: DLS of DAHPS(Y) vs. DAHPS(F).

a) DAHPS(F), b) DAHPS(Y) expressed at 18°C with no IPTG

3.1.3. Unexpected Antibiotic Resistance of *E. coli* BL21(DE3) cells

After multiple trials to reproduce active DAHPS(Y) production at 18°C without IPTG induction, it became apparent that the competent cells used for protein expression had become antibiotic resistant. This included *E. coli* BL21 (DE3) produced in the lab, which were resistant to ampicillin and kanamycin, *E. coli* BL21Star (DE3) cells obtained from another lab, which were ampicillin and kanamycin resistant, and *E. coli* TOP10, which were ampicillin and kanamycin resistant. Antibiotic resistance will undermine protein production since cells that have expelled the plasmid will be able to continue to grow under the expression conditions. Since they no longer have the metabolic cost of producing large amounts of the target protein, they can grow faster and take over the culture. Ultimately, new chemically competent cells from New England Biolabs were able to yield protein.

With these new cells, protein expression at 37°C with IPTG was restored (Figure 29) and DAHPS from *Aeropyrum pernix* could also be expressed at 37°C with IPTG (Figure 30). *A. pernix* is a hyperthermophilic archaeon (archaeon: singular form of archaea) with an optimal growth temperature of up to 100°C⁵⁵, making the enzyme obtained from it optimal for NMR and crystallography.

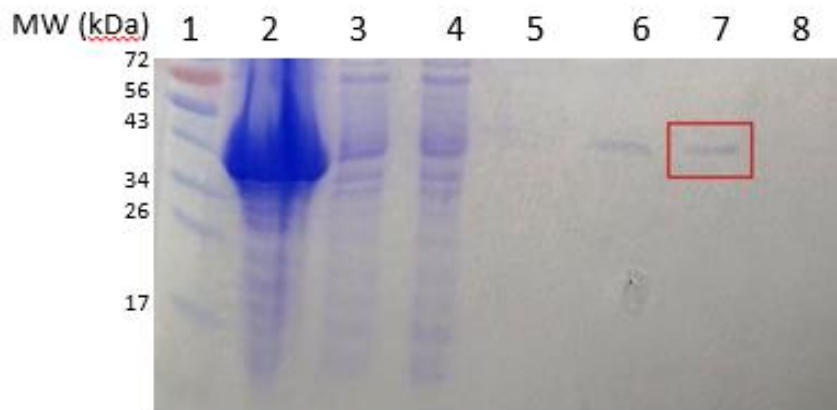


Figure 29: DAHPS(Y) expressed at 37°C with IPTG.

Lanes: 1) molecular weight standards, 2) Filtrate, 3) Run Through from Ni-Sepharose column, 4), 6) – 8) DAHPS(F) purified on Ni-Sepharose Column (lane 5 was blank). The expected molecular weight of DAHPS(Y) is 41 kDa before TEV-tag cleavage.

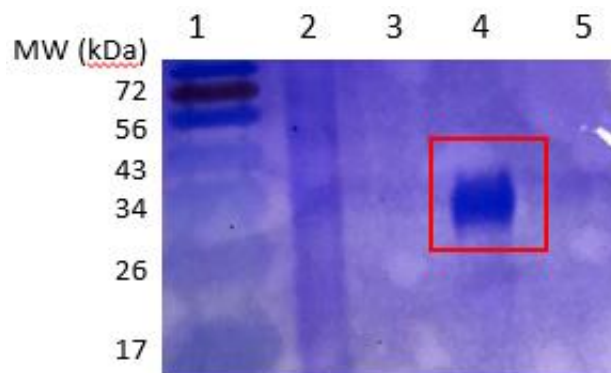


Figure 30: DAHPS from *Aeropyrum pernix* (*A. pernix*) expressed at 37°C with IPTG.

Lanes: 1) molecular weight standards, 2) – 5) DAHPS(F) purified on Ni-Sepharose Column. The expected molecular weight of *A. pernix* DAHPS is 41 kDa.

However, while it was expected that the protein expressed at 37°C with IPTG would not be active, the protein expressed at 18°C without IPTG also showed little to no activity. Finally, the DAHPS from *A. pernix* ended up precipitating out of the buffer solution, also making it inactive.

After this point, we decided to stop troubleshooting further and move forward to the inhibitor design for DAHPS(F).

3.2. Inhibitor Design

Based on the high affinity of DAHP hydrazone for DAHPS(F), and the hypothesis that replacing the water molecule HOH₂ that bridges the hydrazone NH₂ group and the Arg234 sidechain (Figure 14), an inhibitor bearing an *N*-formylhydrazone sidechain was designed. This was first designed as an inhibitor fragment, pyruvate *N*-formylhydrazone (PFH), with the intention of synthesizing DAHP *N*-formylhydrazone if the fragment is effective. PFH was synthesized and tested for its inhibitory activity using the MG/AM assay. The mass spectra and NMR spectra for PFH can be found in Appendix 2.

3.2.1. Pyruvate Formylhydrazone (PFH)

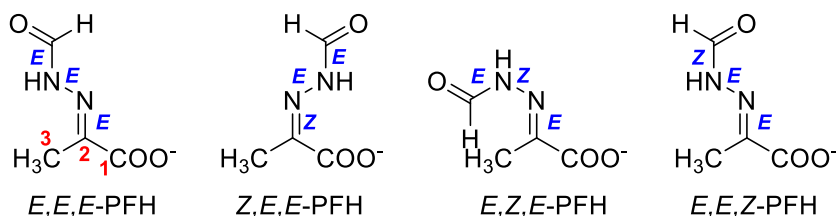
Briefly, PFH was synthesized by reacting pyruvate with formic acid hydrazide in water at room temperature. The reaction was complete as quickly as it could be monitored by NMR. The pyruvate C3H₃ group at 2.41 ppm (Figure 35) and the formic acid hydrazide's H(formyl) proton at 8 ppm (Figure 36) both disappeared, and new sets of peaks at ~2.1 ppm and 8 to 9 ppm

appeared (Figure 37). High resolution mass spectrometry confirmed that the correct mass was present: $m/z = 129.0303$ (obs) versus 129.0306 (calc) (Table 1).

PFH was purified using by anion exchange chromatography on a 1mL Q-Sepharose column using a gradient from 1.6 to 80 mM ammonium acetate, pH 5.5, at 1mL/min for 30 min. PFH eluted between 10-18 min. MS confirmed the presence of the purified product; however, the NMR still displayed multiple peaks.

NMR spectra were run on purified PFH to establish its identity, namely ^1H (Figure 38), ^{13}C (Figure 39), HMBC (Figure 40) and HSQC (Figure 41). It was also run with a standard addition of methanol to determine the yield of 48 mg. Even the purified compound displayed multiple NMR peaks. It is noteworthy that all the peaks were in the range expected for PFH's C_3H_3 (1.9 – 2.2 ppm) and H(formyl) (8 – 9 ppm) protons, that they were all singlets, as expected, and in the 2-D spectra, they all had cross peaks with ^{13}C in the expected ranges. This was ultimately interpreted as being due to multiple isomers of PFH, rather than contaminants. PFH contains one formal $\text{C}=\text{N}$ double bond in the *N*-formyl hydrazone sidechain which could have *E* and *Z* isomers; however, due to extensive resonance stabilization, the other atoms are sp^2 -hybridized, and would be expected to have significant double bond character (Figure 31).

Examples of PFH isomers



Possible isomers

E,E,E	Z,E,E
E,Z,E	Z,Z,E
E,E,Z	Z,E,Z
E,Z,Z	Z,Z,Z

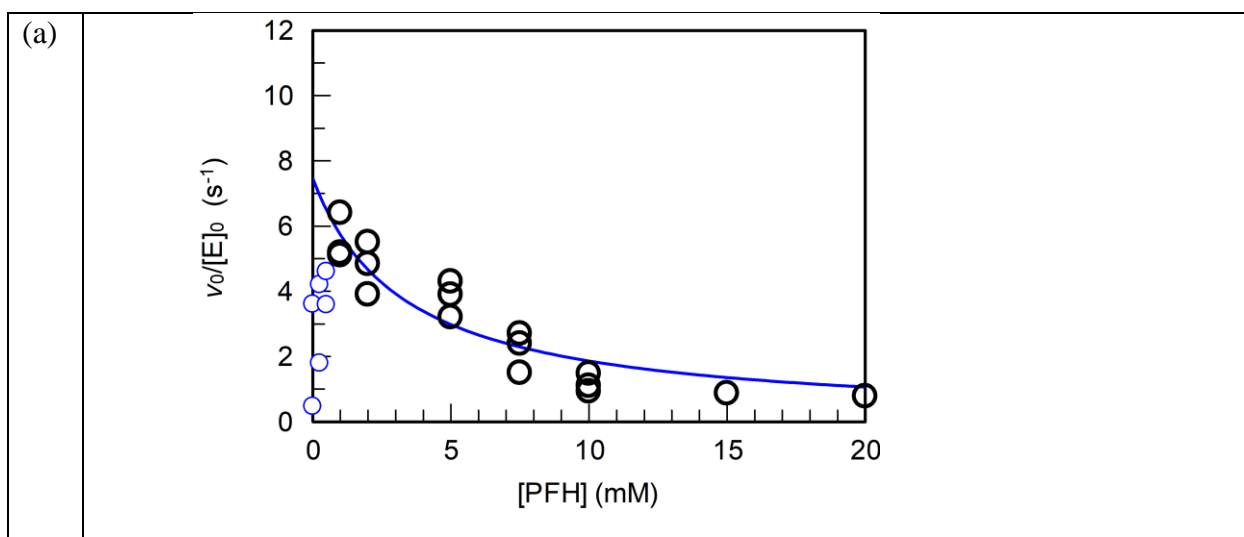
Figure 31. Possible *E* and *Z* isomers of PFH.

A total of eight *E/Z* isomers are possible. Examples at each position are shown (top), and all possible isomers are listed (bottom).

Using a series of computational predictions done by Dr. Berti (Appendix 3), it was determined that the different isomers in the *N*-formylhydrazone side chain have a significant effect on the predicted ^1H and ^{13}C peak positions. Different *E/Z* isomers had C3H_3 chemical shifts of 1.93 to 2.39 ppm compared with the observed peaks at 1.9 to 2.2 ppm. Calculated ^{13}C peaks were 10 – 25 ppm, compared with observed peaks at 11 to 20 ppm. Based on the HSQC spectrum, about 4 major isomers were visualized through the H3-C3 group, and about 3 major isomers were visualized based on the H(formyl)-C(formyl) HSQC. There is only one formal double bond in the *N*-formylhydrazone side chain ($\text{C2}=\text{N2}$), and due to the extensive resonance stabilization within the rest of the side chain, it is not able to rotate as quickly on the NMR timescale, leading to multiple peaks. The isomers around $\text{C2}=\text{N2}$ are configurations and the other bonds would be conformations. However, in this case, these definitions may become clouded because they can likely interchange, but slowly on the NMR timescale.

3.2.2. Inhibitory Assays with PFH using MG/AM Assay

The inhibitory properties of PFH against DAHPS(F) were tested using the MG/AM assay. PFH inhibited DAHPS(F) in both the presence and absence of Gro3P (Figure 32). At very low concentrations PFH caused the initial velocities to increase. This has been observed previously with related inhibitors, though the increases were limited to 10 – 20%; too small to be fitted. In this case, the increases were much larger, but as there is no kinetic model, they were not included in the fit. Instead, only the inhibitory portion of the curve was fitted to equation 1 (Figure 32, black symbols), yielding K_i values of $11 \pm 3 \mu\text{M}$ in the absence of Gro3P, and $6 \pm 3 \mu\text{M}$ with 3 mM Gro3P. The datapoints where PFH was apparently activating DAHPS(F) were not included in the fit (Figure 32, blue symbols). The inhibitory model assumed that inhibition was competitive with respect to PEP and E4P, and noncompetitive with respect to Mn^{2+} , as would be expected by analogy to the pyruvate oxime + Gro3P and glyoxylate + erythritol 4-phosphate pairs characterized previously⁵.



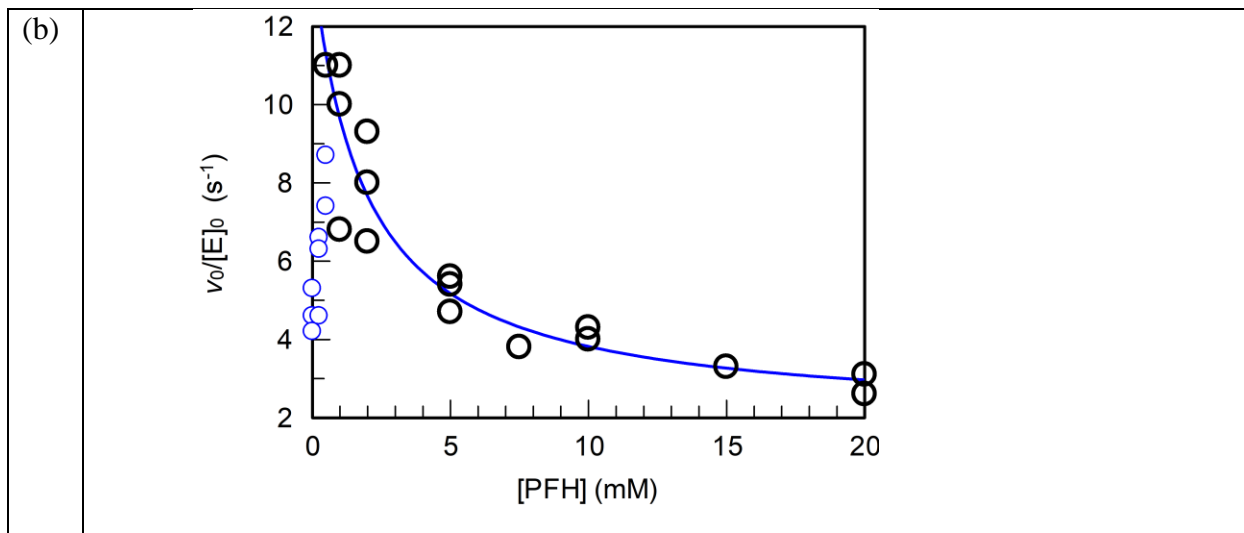


Figure 32: PFH inhibition of DAHPS(F)

Black symbols indicate initial velocities fitted to equation 1. Blue symbols indicate initial velocities at low PFH concentrations that were excluded from the fit because of apparent enzyme activation. (a) without Gro3P, $K_i = 11 \pm 3 \mu\text{M}$, $k_{\text{cat}(\text{apparent})} = 10 \pm 1 \text{ s}^{-1}$ (b) with 3 mM Gro3P, $K_i = 6 \pm 3 \mu\text{M}$, $k_{\text{cat}(\text{apparent})} = 16 \pm 2 \text{ s}^{-1}$. The source of the discrepancy in $k_{\text{cat}(\text{apparent})}$ values is not known.

3.2.3. DAHP Synthesis and Purification

DAHP was synthesized as a precursor for DAHP *N*-formylhydrazone as described previously⁴², and was purified using anion exchange chromatography on a Q-Sepharose column running a gradient from 0.1 to 0.8 M ammonium formate at 1mL/min. The fractions were tested for the presence of E4P using the RSA and the chromatograph measuring at 230 nm was used to determine the presence of PEP. The fractions in between were tested using the APase assay to determine the presence and concentration of DAHP. According to the RSA, the E4P fractions eluted between 6-8 min, while using the APase assay, the DAHP eluted between 9-12 min. Using the chromatograph, it was also found that PEP elutes between 14-16 min. The concentration of

DAHP was determined by taking varying aliquot sizes and determining the P_i content in a 10-fold diluted sample after reaction with APase (Figure 33).

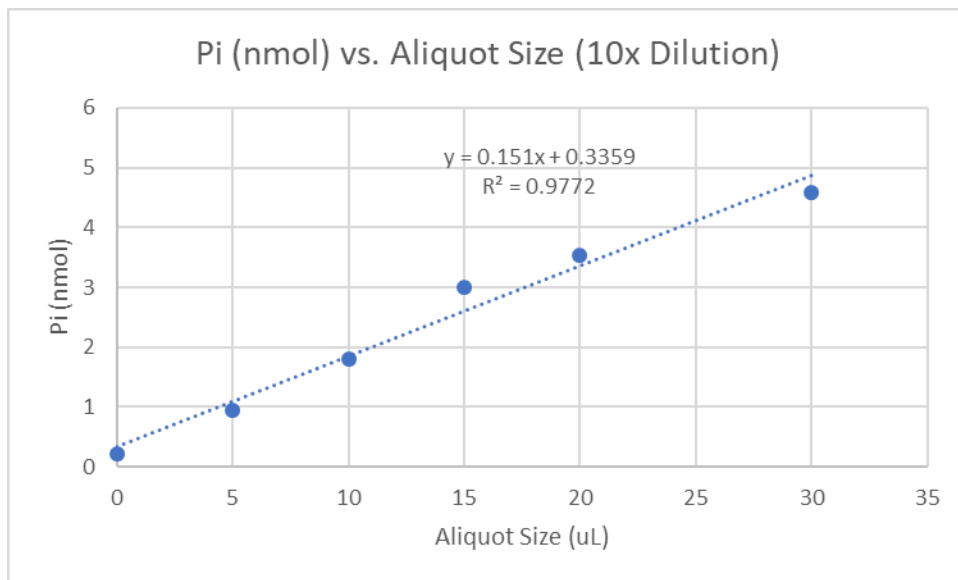


Figure 33: Pi(nmol) vs. Aliquot Size (10x dilution) for DAHP

Determined the concentration of DAHP in the stock solution by calculating the amount of P_i (nmol) per μL of sample.

Yield of DAHP after purification was $7.6 \mu\text{mol}$, while the theoretical yield was $20 \mu\text{mol}$, assuming E4P as the limiting reagent.

4. Discussion

4.1. Protein Dynamics

4.1.1. DAHPS(Y) Troubleshooting

After multiple attempts to produce active DAHPS(Y), and in spite of the fact that it had been produced previously in an active form by our group (N. Balachandran, personal communication) and others⁵⁶, it was not possible to produce active DAHPS(Y). The fact that it was possible to produce active DAHPS(F) using the same expression and purification methods argues against any significant errors in the methods, or problems with the reagents used. Some problems were unearthed in the process of troubleshooting DAHPS(Y) production, including the discovery that several lab strains of *E. coli* had acquired resistance to the antibiotics used to select for the DAHPS(Y) plasmid. While these problems were eventually corrected, the fundamental problem remained that DAHPS(Y) was inactive. DLS experiments revealed that the protein was insoluble and aggregated during expression in the cells, during purification and / or during the DLS experiments themselves. Sequentially collected DLS spectra on the same sample demonstrated increasing aggregation over time (Figure 22). DLS established that the lack of DAHPS(Y) activity was due to aggregation and precipitation, though not why these problems were occurring. It was useful, though, in helping minimize the problem.

4.1.2. Troubleshooting Purification Conditions

DAHPS(Y) was treated with reagents that have been shown previously to help with protein stability in general, namely MgCl₂, TCEP and Arg+Glu, and DAHPS(Y) specifically, namely MgCl₂ (N. Balachandran, personal communication). MgCl₂ helps stabilize the protein

using nonspecific electrostatic forces³¹. DAHPS requires a divalent metal cation for activity, and while Mg^{2+} can stabilize DAHPS, it is not one of the metals that is able to activate it³². However, it is expected that in the absence of other divalent metal cations Mg^{2+} would be able to bind in DAHPS's metal binding site to help stabilize the protein. Based on DLS spectra, a 24 h incubation with $MgCl_2$ helped reduce the aggregation of purified protein (Figure 23). TCEP is an antioxidant that is capable of reducing disulfide bonds to cysteine residues, and previous studies have shown that it helps with protein solubility^{33,34}. Based on DLS, a 24 h incubation with TCEP did increase the solubility of the purified protein (Figure 24). Surprisingly, incubating DAHPS(Y) for 24 h with both $MgCl_2$ and TCEP did not reduce aggregation (Figure 25). The reason for this is not known, but based on work done by previous students, different ratios may show different results.

Glutamic acid and arginine together (50 mM each) has previously shown increased protein solubility and stability in other proteins³⁵. Arginine has been shown to improve the refolding of recombinant proteins in *E. coli* within inclusion bodies by suppressing the aggregation of folding intermediates during thermal unfolding or refolding through three mechanisms³⁶. However, based on DLS, the protein solubility did not improve after a 24-h treatment in the case of DAHPS(Y) (Figure 26).

Based on this information, the purification conditions were altered. Three different methods for purification that had previously yielded active DAHPS(Y) were tested. It was found that when TCEP and $MgCl_2$ were added in each step in a 1:3 ratio, the protein was least aggregated, although the protein was still inactive.

4.1.3. Troubleshooting Expression Conditions

DAHPS(Y) was then expressed at 37°C with and without IPTG and at 18°C with and without IPTG, and there was temporary activity observed when the protein was expressed at 18°C without IPTG until the His-tag was removed. DLS was used to test for aggregation, and it was found that the diameter of DAHPS(Y) was approximately half of DAHPS(F), which is expected (Figure 28).

4.1.4. *Aeropyrum pernix* DAHPS

Given the problems with producing active DAHPS(Y), a more thermostable DAHPS was produced. *A. pernix* is a thermostable archaea that is able to grow at temperatures between 90°C to 95°C, and DAHPS from *A. pernix* has been previously been expressed successfully in *E. coli*⁵⁷. Based on this, it was predicted that the DAHPS from *A. pernix* would be more likely active and all further experiments would be done with it. However, when we tried to express and purify the protein, the protein was too concentrated, and it precipitated out of solution. Therefore, the project was discontinued and will be revisited at a future time.

4.2. Inhibitor Design

4.2.1. PFH Synthesis and Testing

PFH was synthesized by reacting sodium pyruvate with formic acid hydrazide and using the LDH assay to monitor the consumption of pyruvate. NMR and high-resolution MS was done to observe the purity of the product. Multiple product peaks were observed by NMR in both the crude product and purified PFH. By HSQC 2-D NMR spectroscopy, there were 3 – 4 major species present. These multiple peaks appear to originate in the *E/Z* isomerization of PFH. Up to

8 possible isomers were characterized using quantum mechanical optimizations, and the predicted chemical shifts matched well with the observed values (Figure 44, Appendix 3). The agreement between predicted and observed chemical shifts and the correct m/z value by high resolution mass spectrometry served to confirm the identity of the product PFH.

When the PFH was tested as a DAHPS(F) inhibitor, it activated the enzyme at very low concentrations, but inhibited it at high concentrations. A similar effect has been observed previously with oxime-based inhibitors of KDO8PS and NeuB, though in those cases activation was on the order of 10 – 20%. The source of this activation is not known, but one possible cause relates to the effects of inhibitor binding to different subunits. DAHP oxime inhibition of DAHPS(F) was characterized by positive cooperativity of inhibitor and substrate binding⁴. That is, DAHP oxime binding to half the subunits of homotetrameric DAHPS(F) caused substrate binding to increase at least 10-fold. If the same kinetic mechanism is occurring with PFH, then initial inhibitor binding could lead to increased rates as substrate binding improves, followed by inhibition as all the subunits become occupied by inhibitor. This preliminary explanation will have to be confirmed. Whatever the cause of the increase in initial velocities, PFH displayed significant inhibition at higher concentrations in both the absence and presence of Gro3P, with apparent K_i values of $11 \pm 3 \mu\text{M}$ and $6 \pm 3 \mu\text{M}$, respectively. In comparison, pyruvate oxime did not inhibit DAHPS(F) in the absence of Gro3P and had an apparent K_i of 1.3 mM in its presence. Pyruvate hydrazone, in contrast, inhibits DAHPS(F) with an apparent K_i value of $30 \mu\text{M}$ in the presence of Gro3P (M. Peng and M. Heimhalt, personal communication). Thus, PFH is an inhibitor at least on par with pyruvate hydrazone. Its true affinity could be higher than the K_i values suggest because the conformer of the *E/Z* isomer that binds DAHPS(F) may be only a fraction of the total PFH concentration. This validates the approach of adding an oxygen atom to

the inhibitor in place of a water molecule observed in the crystal structure, though only complete characterization of the full-size inhibitor, DAHP *N*-formylhydrazone, will be required to definitively demonstrate whether this is true. The full-length DAHP-based inhibitor for PFH is now ready to be synthesized and tested.

4.3. Future Directions

4.3.1. Protein Dynamics

Because of the issues that have been observed in producing active enzyme, we have decided to not pursue the protein dynamics of DAHPS(Y) any further but may revisit this later. If it still leads to issues, expression of the hyperthermophilic *A. pernix* DAHPS will be repeated. This will not only be beneficial for the expression; it will also be ideal for the NMR and crystallization conditions.

After completing any required troubleshooting, 5-fluoroindole labelled DAHPS will be expressed to run ^{19}F NMR on the protein. The NMR will be done in collaboration with Dr. Scott Prosser at the University of Toronto, Mississauga. The purpose of the ^{19}F NMR is to better understand the structure and functionality of the DAHPS. Nudge mutations will also be used to identify which peaks correspond to the Trp residues in the NMR spectrum. Expressing DAHPS(Y) with a V235I mutation will be the first mutation that will be looked at.

4.3.2. Inhibitor Design

As of now, PFH has been tested and we have confirmed that it does have inhibitory effects. The next step is to synthesize the full-size inhibitor, DAHP *N*-formylhydrazone. If this

proves to be an effective inhibitor, the corresponding *N*-formylhydrazone derivatives of KDO8P and NeuNAc will be synthesized and tested as inhibitors of KDO8PS and NeuB, respectively.

5. Appendix

5.1. Appendix 1 – Mass Spectrum of DAHPS(Y)

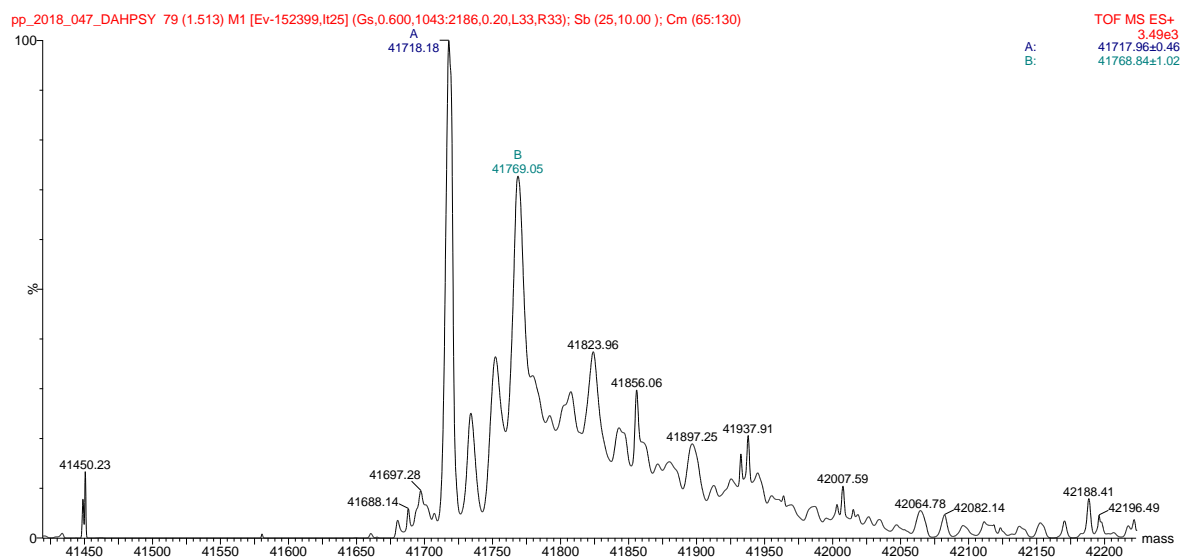


Figure 34: Mass spectrum of DAHPS(Y).

The observed molecular weight was 41,718 Da versus the calculated value of 41,719 Da. The higher molecular weight peaks at intervals of $m/z = 17$ are likely ammonium ion adducts, as the protein was prepared in 10mM ammonium acetate.

5.2. Appendix 2: NMR and Mass Spectra for Pyruvate, FAH, and PFH

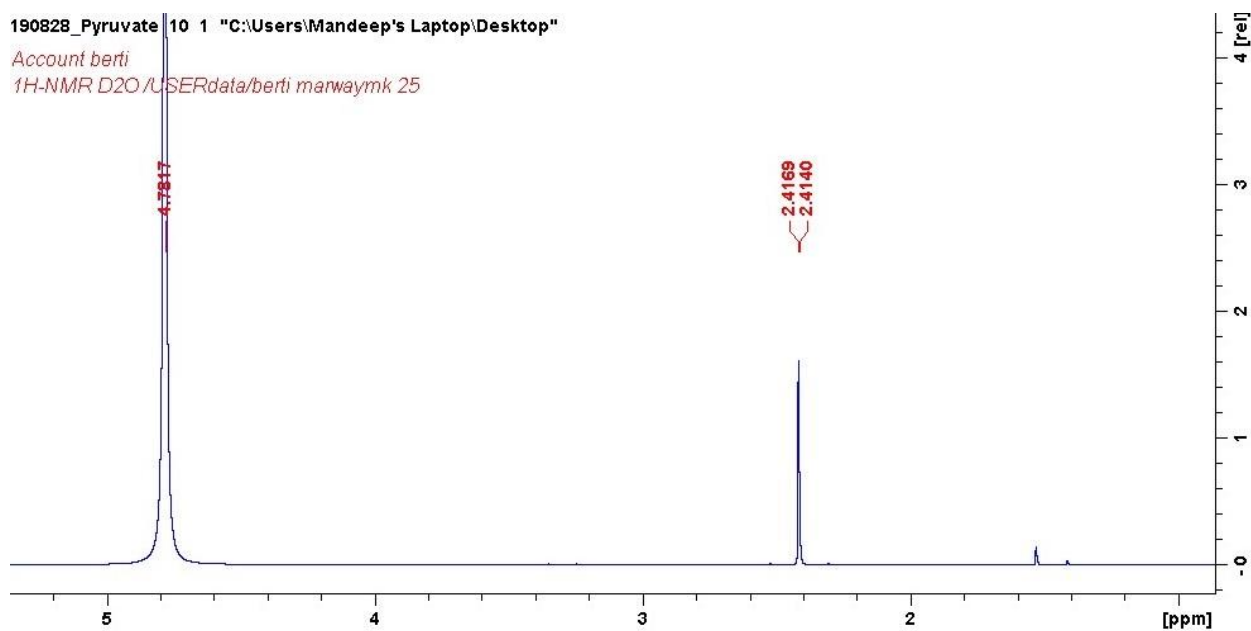


Figure 35: $^1\text{H-NMR}$ for pyruvate acquired using the 600MHz NMR.

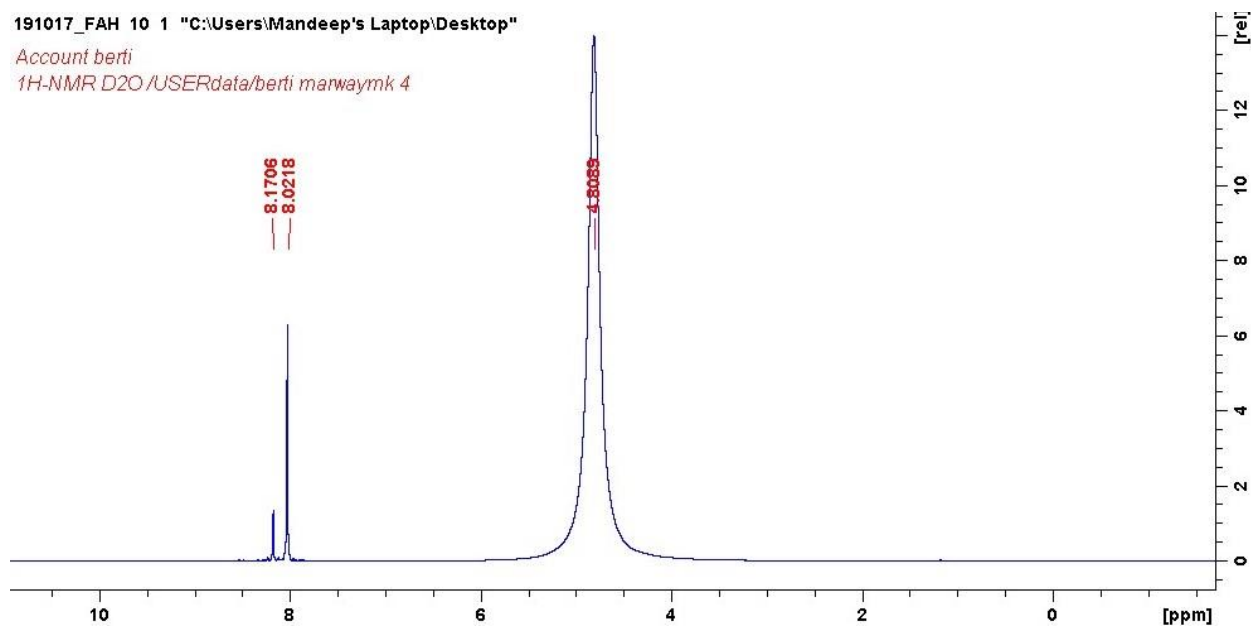


Figure 36: $^1\text{H-NMR}$ for FAH acquired using the 600MHz NMR.

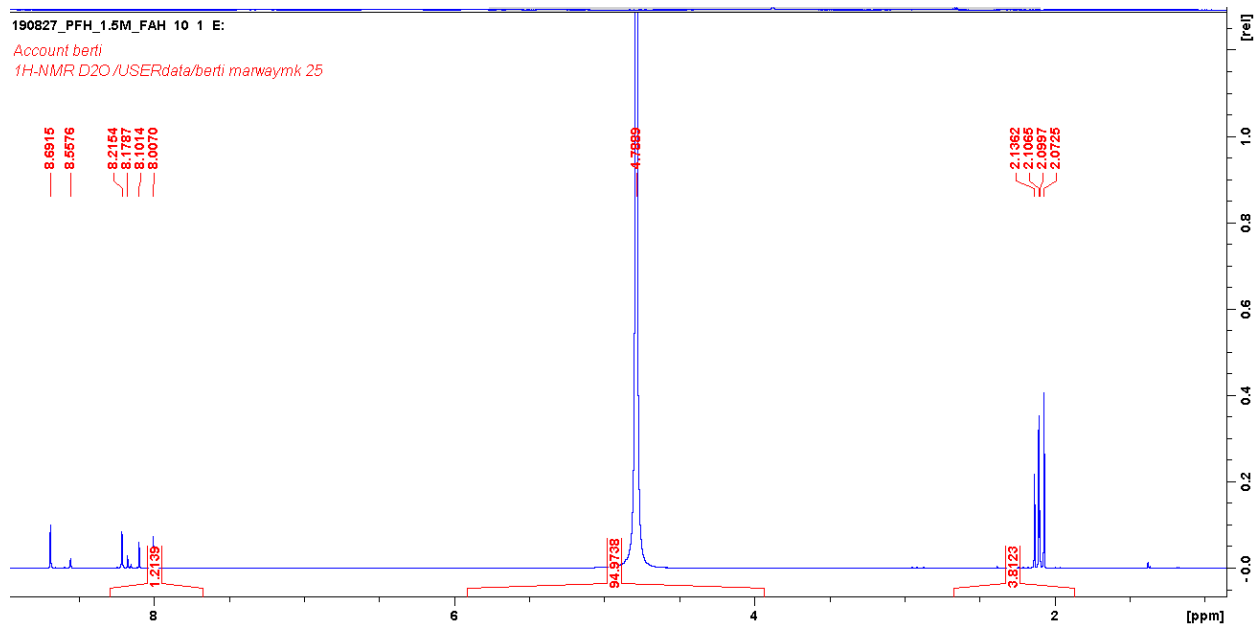


Figure 37: $^1\text{H-NMR}$ for crude Pyruvate-*N*-Formylhydrazone (PFH) acquired using the 600MHz NMR.

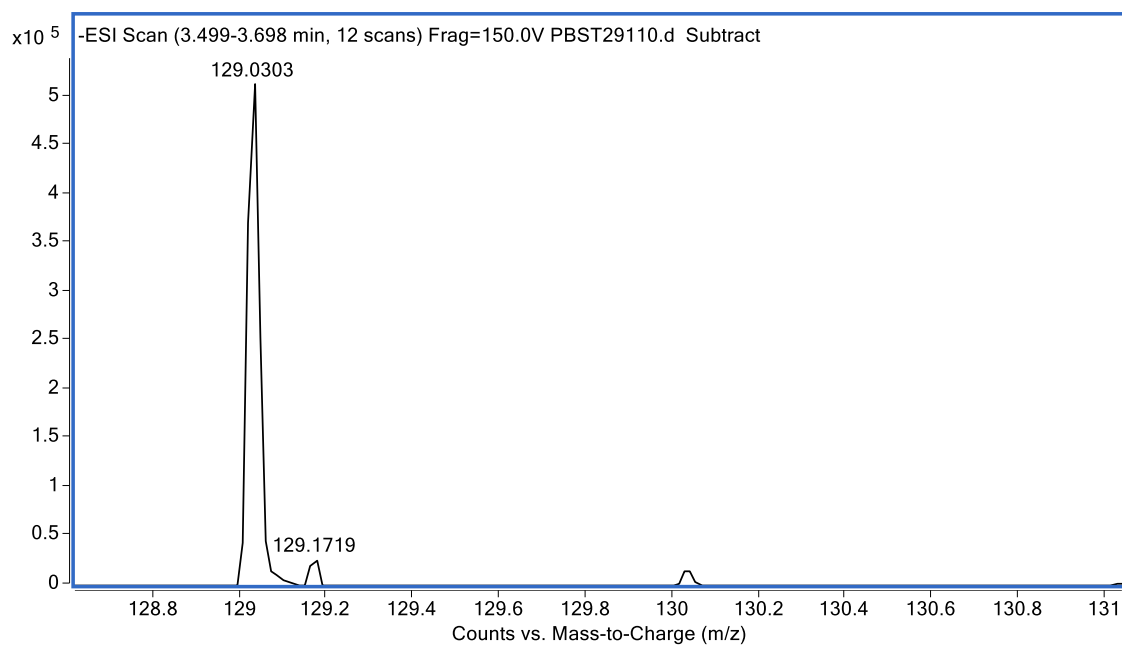
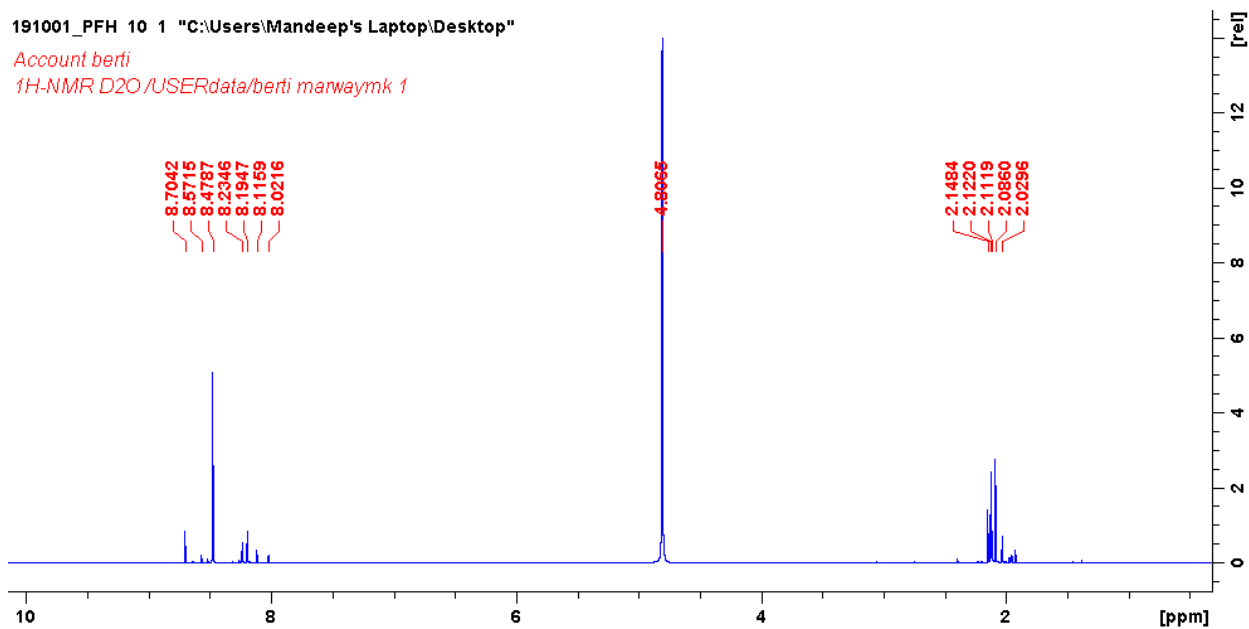


Figure 38: High-Resolution MS for crude PFH.**Table 1:** Tabulated results for MS for crude PFH.

Formula (M)	Score	Mass	Calc Mass	Calc m/z	Diff (ppm)	DBE	m/z
$C_4H_6N_2O_3$	99.99	130.0376	130.0378	129.0306	2.04	3	129.0303

**Figure 39:** 1H -NMR for purified Pyruvate-*N*-Formylhydrazone (PFH) acquired using the 600MHz NMR.

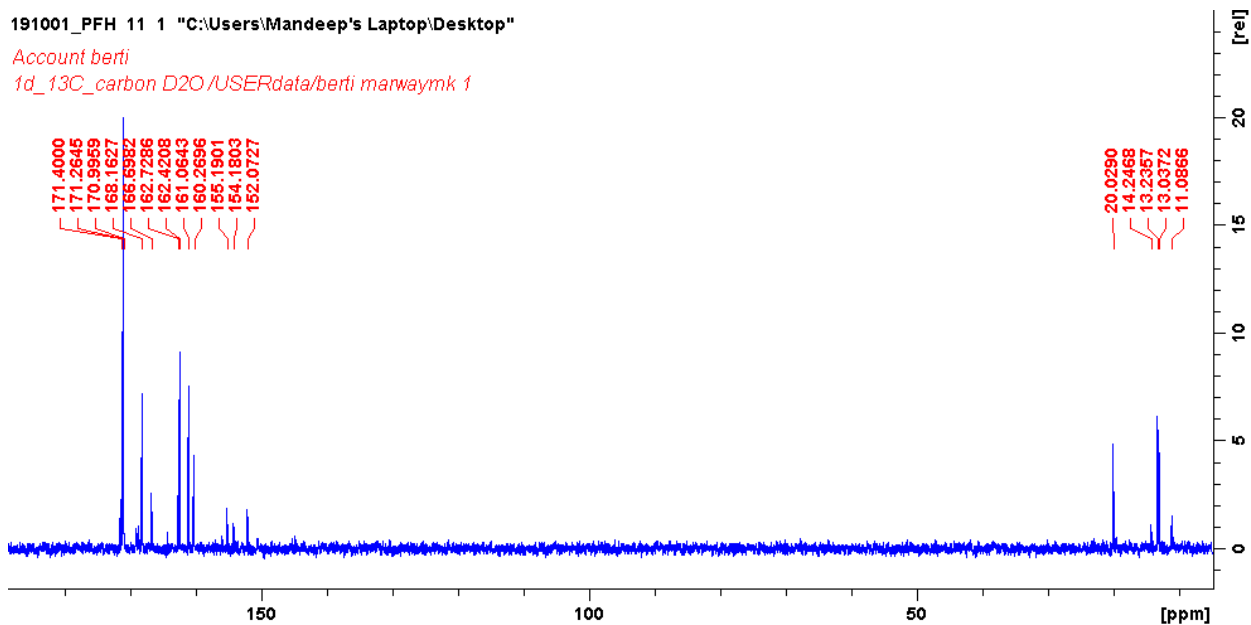


Figure 40: ^{13}C -NMR for purified Pyruvate-*N*-Formylhydrazone (PFH) acquired using the 600MHz NMR.

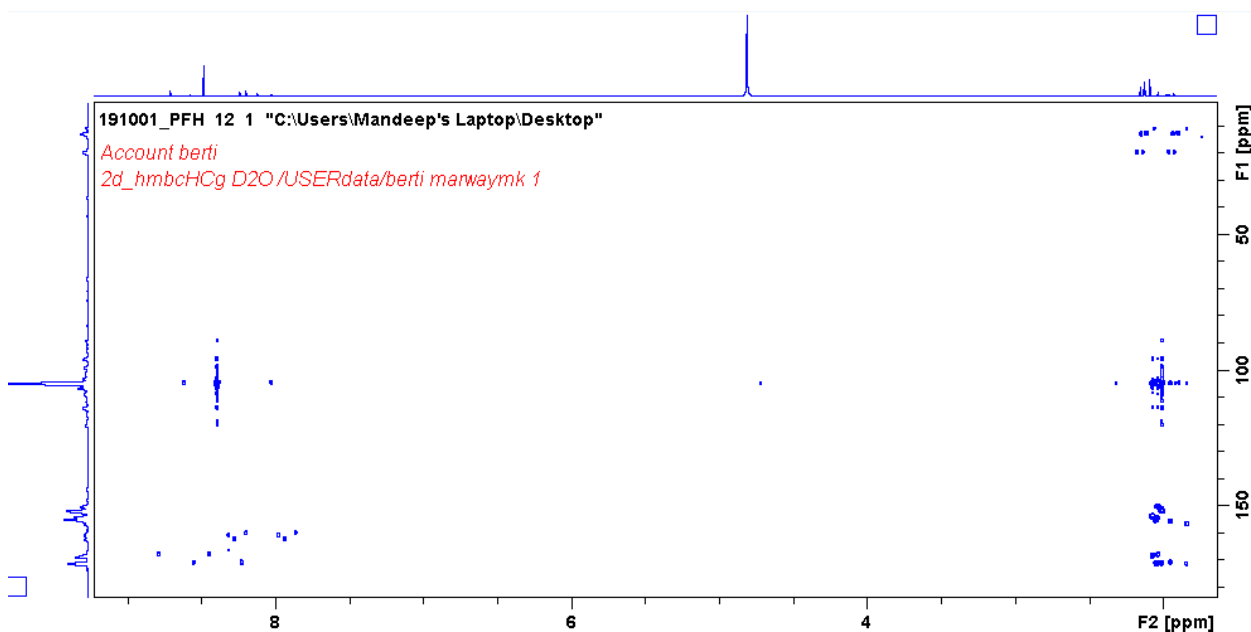


Figure 41: HMBC NMR for purified Pyruvate-*N*-Formylhydrazone (PFH) acquired using the 600MHz NMR.

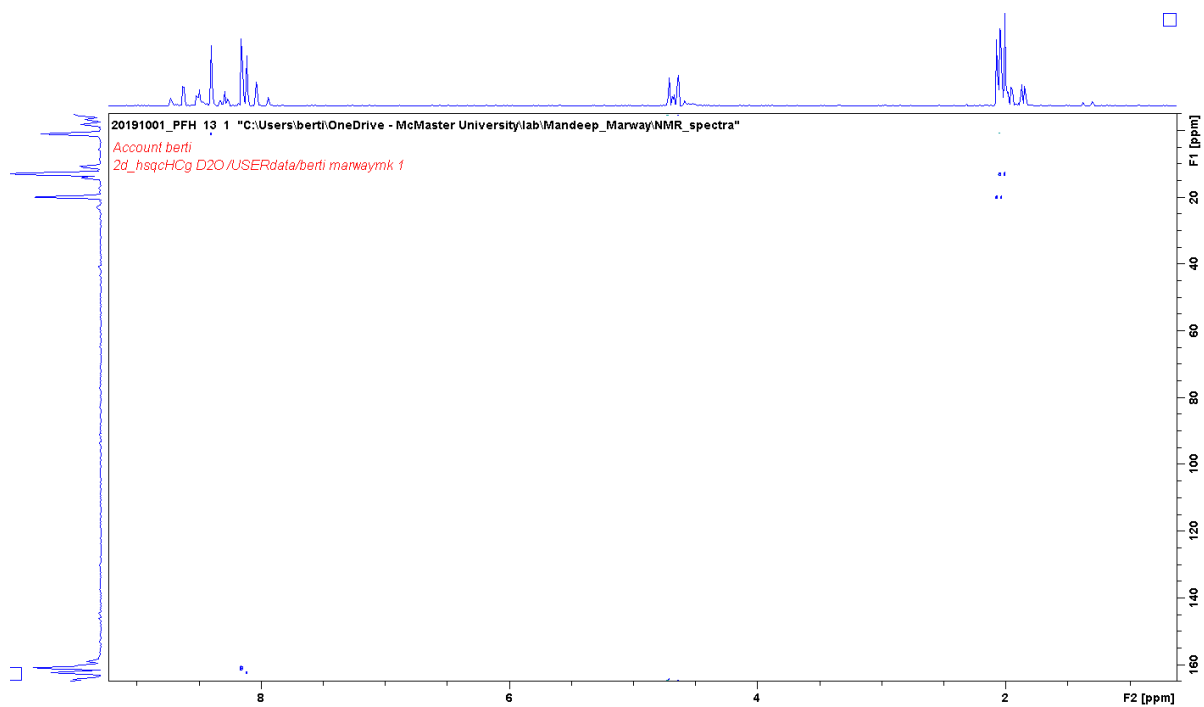


Figure 42: HSQC NMR for purified Pyruvate-*N*-Formylhydrazone (PFH) acquired using the 600MHz NMR.

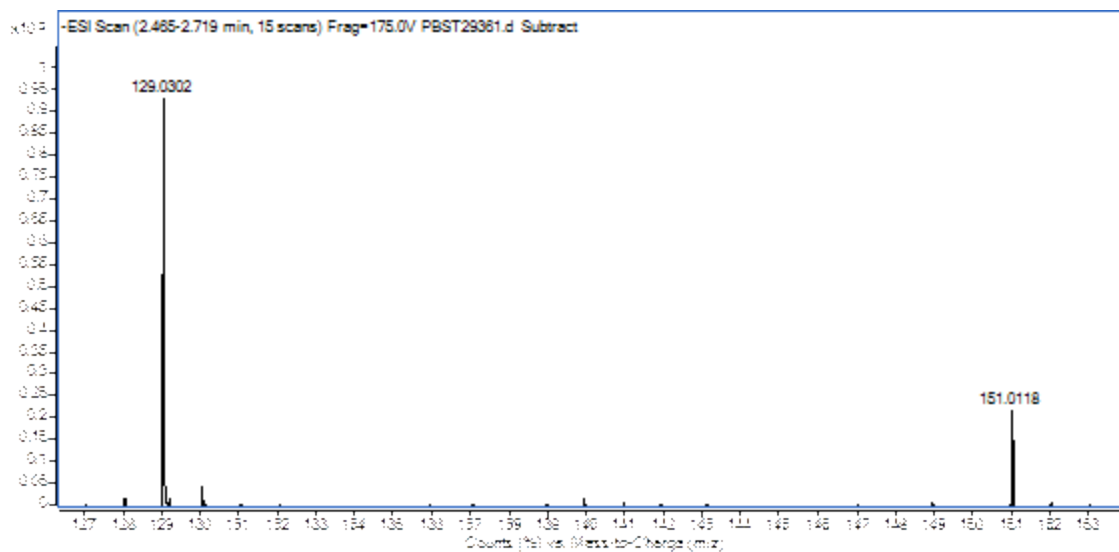


Figure 43: High-Resolution MS for purified PFH.

Table 2: Tabulated results for MS for purified PFH.

Formula (M)	Score	Mass	Calc Mass	Calc m/z	Diff (ppm)	DBE	m/z
C4 H6 N2 O3	99.98	130.0375	130.0378	129.0306	2.81	3	129.0302

5.3. Appendix 3 – Computational prediction of PFH NMR chemical shifts

(Computations and analysis performed by Paul Berti)

5.3.1. Summary

A series of computations to predict the NMR spectra of PFH show that different isomers in the *N*-formylhydrazone side chain have significant effects on the predicted ^1H and ^{13}C peak positions. Because of the uncertainty of the protonation state and relative contributions of different isomers, it is difficult to make more precise predictions. However, the range of predicted ^1H peak positions was large (1.93 - 2.39 ppm), as well as ^{13}C peaks (9.7 - 25 ppm). Therefore, it is reasonable to expect multiple peaks in the experimental NMR spectra. Based on the HSQC spectrum, there appears to be about 4 major isomers present (based on H3-C3 HSQC), or 3 isomers (based on H(formyl)-C(formyl)). Since the latter group is isolated from the rest of the molecule, it's possible that the different isomers lead to overlapping peaks in the formyl group's HSQC spectrum.

Strictly speaking, there is only one double bond in the formylhydrazone side chain (C2=N2); however, due to extensive resonance stabilization in the rest of the side chain, the rest of the side chain is expected not to rotate quickly on the NMR time scale, leading to multiple peaks. Strictly speaking, the isomers around C2=N2 are configurations and around the other

bonds are conformations, but the definitions become clouded in this case because they can all likely interchange, but slowly on the NMR timescale.

5.3.2. Rationale

The ^1H and ^{13}C NMR spectra of (apparently pure) PFH show multiple peaks. It is possible that this is because of changes in *N*-formylhydrazone sidechain's conformations/configurations that are slow on the NMR timescale. The only formal double bond is $\text{C}2=\text{N}2$, but the formamide ($\text{H}(\text{C}=\text{O})\text{-NH}$) and N-N bonds likely also have significant double bond character.

We therefore examined the effects of different configuration/conformations by calculating the expected chemical shifts for each isomer.

Each structure was optimized using Gaussian 16 at the RB3PW91/6-31+G** level of theory either in vacuum, or using continuum solvation to mimic water:

```
# rb3pw91/6-31+G** OPT guess=read geom=checkpoint test
#SCRF(CPCM,read,solvent=water) NoSymm
[...]
radii=ua0 SphereOnAcidicHydrogens

then

# rb3pw91/6-31+G** guess=read geom=checkpoint NMR test
```

This was done on the COOH (vacuum, SCRF) and COO⁻ (SCRF) forms of PFH.

Trying to optimize the middle group as the Z isomer (the N-N bond) caused clashes with other groups and dihedral angles of approx. -40° to -70° . ZZZ was unstable in the COO- form, and optimized to the ZEZ isomer.

The dominant isomers depend on the protonation state of the C1 carboxyl group, depending on whether there is a hydrogen bond between $\text{COOH}\cdots\text{N2}$ (COOH form) or $\text{COO}^-\cdots\text{N3H}$ (COO- form).

	Relative energy (kcal/mol)		
Isomer	COOH-vacuum	COOH-scrf	COO--scrif
<i>EEE</i>	0.0	0.0	5.8
<i>EEZ</i>	2.0	1.1	7.3
<i>EZE</i>	6.0	8.2	12
<i>EZZ</i>	4.6	6.1	11
<i>ZZZ</i>	13	13	-*
<i>ZZE</i>	13	16	11
<i>ZEZ</i>	13	12	1.2
<i>ZEE</i>	9.3	10.5	0.0

* Optimized to the ZEZ isomer.

COOH form - scrif		
EEE	EEZ	EZE

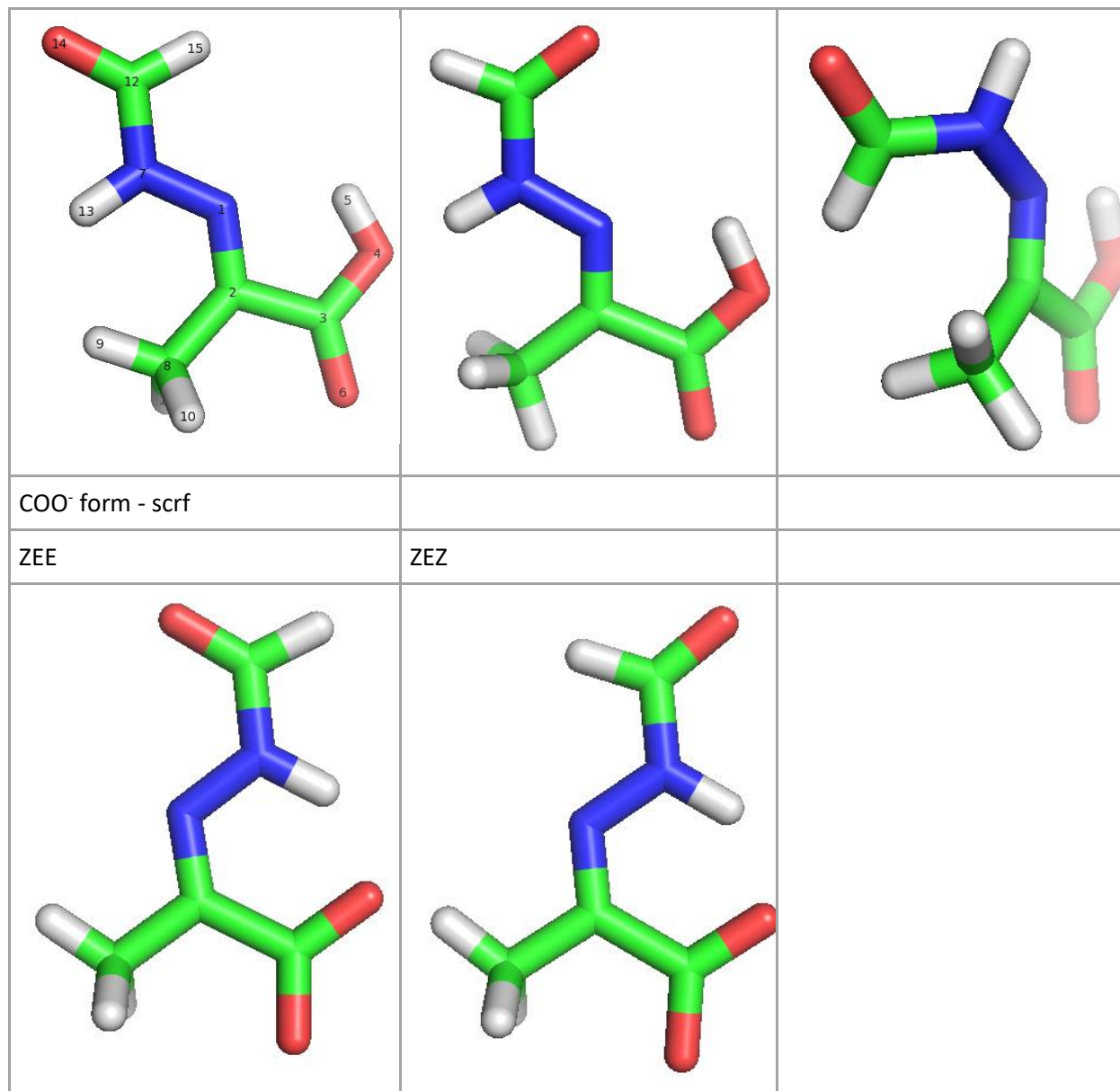


Figure 44: 8 possible isomers characterized using quantum mechanical optimizations

Based on the HSQC 2-D NMR spectrum, there are 3-4 major species present. Figure prepared by Dr. Berti.

5.3.3. Chemical shift trends

H3, C3

The smallest chemical shift is associated with the most favourable isomer for each protonation state. As expected, the chemical shifts are lower for COO⁻, as carboxylates are electron donating, while carboxylic acids are electron withdrawing.

There was quite a good correlation between energy and chemical shift for H3 and C3 for COOH, with increased energy corresponding to a larger chemical shift. (see, e.g., graph for COOH_scrf for H3). The general trend occurs for H3 in COO⁻ form, but not C3.

The range of H3 chemical shifts was 1.93 - 2.39 ppm. Leaving out the highest energy species (> 10 kcal/mol relative energy), the range was 1.93 - 2.27 ppm.

The range of C3 chemical shifts was 10 - 25 ppm.

5.3.4. Predicted chemical shifts (ppm)

COOH_scrf.

	H3	C3	C1	C2	C(formyl)	H(formyl)
<i>EEE</i>	2.11	10.2	161	140	162	8.9
<i>EEZ</i>	2.11	9.7	162	141	155	8.4
<i>EZE</i>	2.27	16.4	162	149	158	8.8
<i>EZZ</i>	2.09	18.7	161	158	152	8.3
<i>ZZZ</i>	2.39	24.4	159	162	156	8.4
<i>ZZE</i>	2.38	24.6	159	160	160	8.0

<i>ZEZ</i>	2.29	23.1	161	144	154	8.2
<i>ZEE</i>	2.25	23.1	161	142	162	8.8

COO⁻_scrif

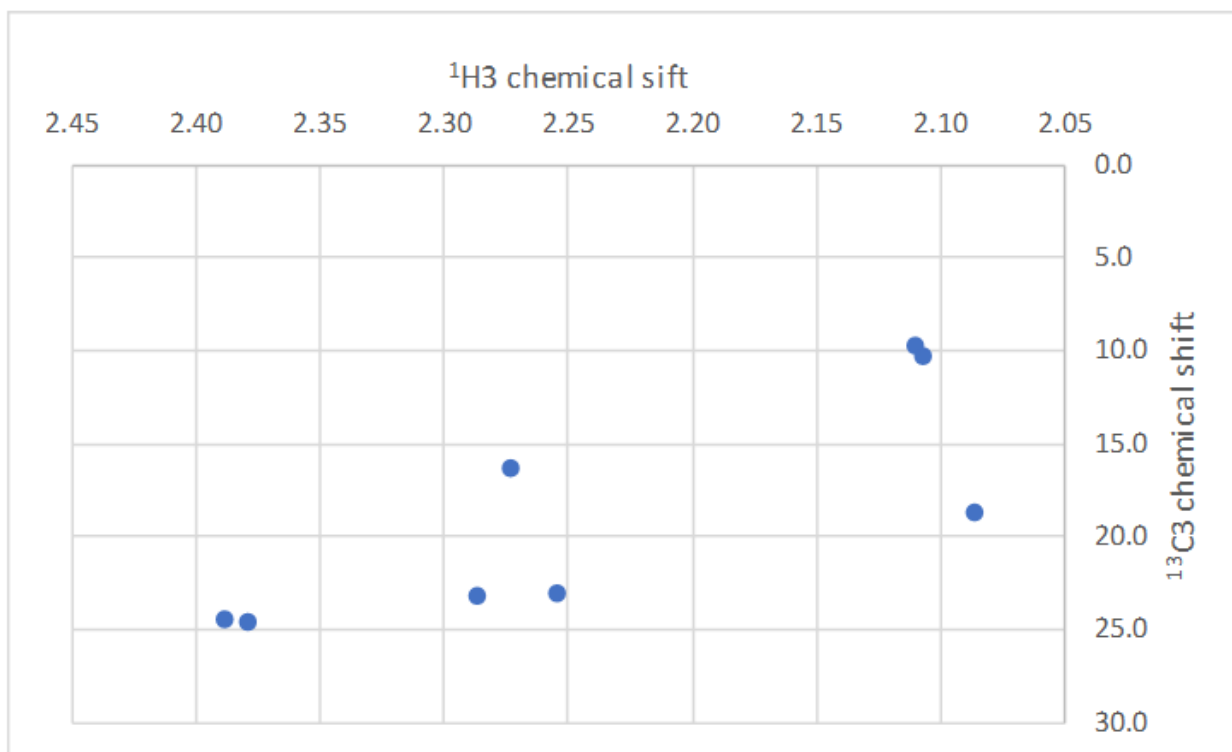
	H3	C3	C1	C2	C(formyl)	H(formyl)
<i>EEE</i>	2.11	13.2	164	152	162	8.9
<i>EEZ</i>	2.12	12.7	164	153	154	8.3
<i>EZE</i>	2.13	17.4	169	175	159	8.1
<i>EZZ</i>	2.01	19.9	169	178	152	8.2
<i>ZZZ</i>						
<i>ZZE</i>	2.11	24.2	167	174	160	8.7
<i>ZEZ</i>	1.98	25.2	164	150	154	8.2
<i>ZEE</i>	1.93	25.0	164	148	162	8.7

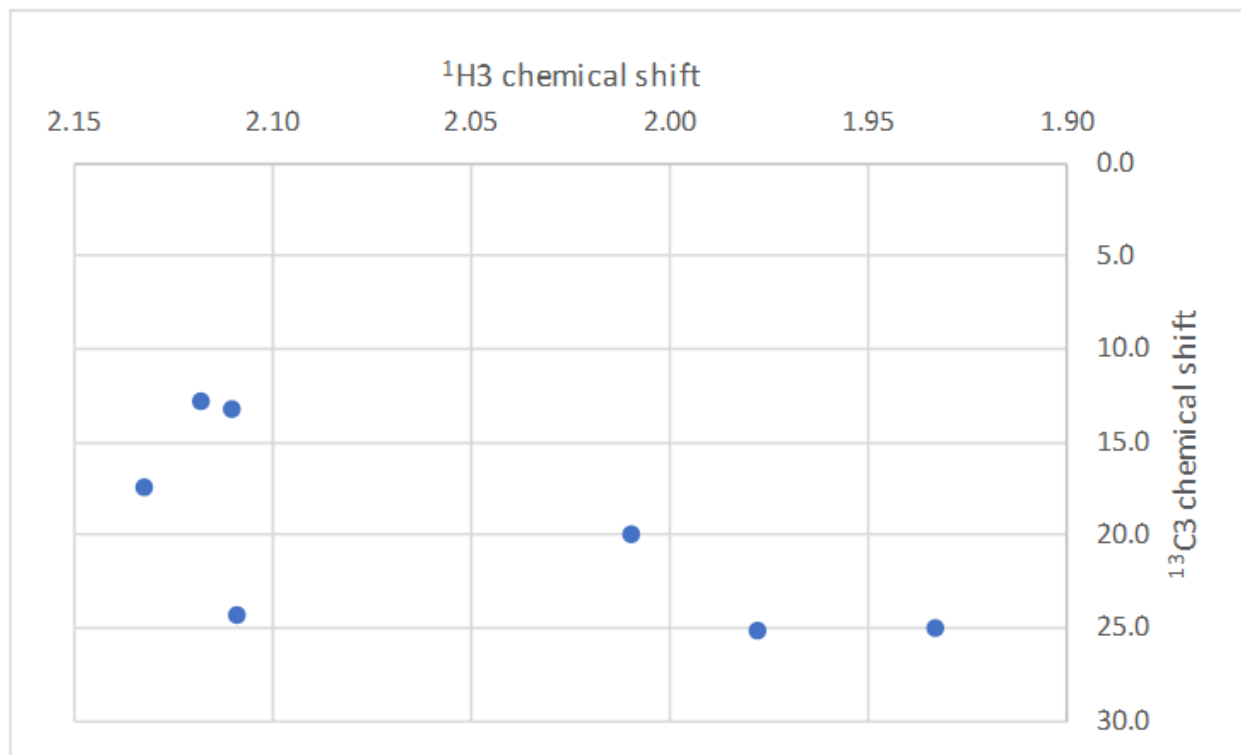
COOH_vacuum

	H3	C3	C1	C2	C(formyl)	H(formyl)
<i>EEE</i>	1.91	11.7	157	137	157	8.8
<i>EEZ</i>	1.96	8.4	158	138	148	8.3
<i>EZE</i>	2.21	16.2	157	148	153	8.7
<i>EZZ</i>	2.19	18.3	157	160	148	8.2
<i>ZZZ</i>	2.35	24.1	154	164	152	8.4
<i>ZZE</i>	2.33	23.9	155	159	159	8.0
<i>ZEZ</i>	2.25	22.1	156	141	148	8.2
<i>ZEE</i>	2.20	22.3	155	139	158	8.8

5.3.5. Predicted peak positions

COOH_scrf



COO-_scrif

References

- (1) Llor, C.; Bjerrum, L. Antimicrobial Resistance: Risk Associated with Antibiotic Overuse and Initiatives to Reduce the Problem. *Ther. Adv. Drug Saf.* **2014**, *5*, 229–241.
- (2) de Kraker, M. E. A.; Stewardson, A. J.; Harbarth, S. Will 10 Million People Die a Year Due to Antimicrobial Resistance by 2050? *PLOS Med.* **2016**, *13*, e1002184.
- (3) Herrmann, K. M.; Weaver, L. M. The Shikimate Pathway. *Annu. Rev. Plant Physiol. Plant Mol. Biol.* **2002**, *50*, 473–503.
- (4) Balachandran, N.; Heimhalt, M.; Liuni, P.; To, F.; Wilson, D. J.; Junop, M. S.; Berti, P. J. Potent Inhibition of 3-Deoxy-d-Arabinohexulose-7-Phosphate (DAHPh) Synthase by DAHP Oxime, a Phosphate Group Mimic. *Biochemistry* **2016**, *55*, 6617–6629.
- (5) Heimhalt, M.; Jiang, S.; Berti, P. J. Eliminating Competition: Characterizing and Eliminating Competitive Binding at Separate Sites between DAHP Synthase's Essential Metal Ion and the Inhibitor DAHP Oxime. *Biochemistry* **2018**, *57*, 6679–6687.
- (6) Maeda, H.; Dudareva, N. The Shikimate Pathway and Aromatic Amino Acid Biosynthesis in Plants. *Annu. Rev. Plant Biol.* **2012**, *63*, 73–105.
- (7) Park, O. K.; Bauerle, R. Metal-Catalyzed Oxidation of Phenylalanine-Sensitive 3-Deoxy- D - Arabino -Heptulosonate-7-Phosphate Synthase from Escherichia Coli : Inactivation and Destabilization by Oxidation of Active-Site Cysteines. **1999**, *181*, 1636–1642.
- (8) Zucko, J.; Dunlap, W. C.; Shick, J. M.; Cullum, J.; Cercelet, F.; Amin, B.; Hammen, L.; Lau, T.; Williams, J.; Hranueli, D.; et al. Global Genome Analysis of the Shikimic Acid Pathway Reveals Greater Gene Loss in Host-Associated than in Free-Living Bacteria. *BMC Genomics* **2010**, *11*, 628.
- (9) Yep, A.; Grmai, L.; Emanuele, A. A.; Woodard, R. W. An Unassigned DAHP Synthase Activity Found Only in Pathogenic Escherichia Coli Strains. *FASEB J.* **2011**, *25*.
- (10) McConkey, G. A. Targeting the Shikimate Pathway in the Malaria Parasite Plasmodium Falciparum. *Antimicrob. Agents Chemother.* **1999**, *43*, 175–177.
- (11) Nirmal, C. R.; Rao, R.; Hopper, W. Inhibition of 3-Deoxy-D-Arabinohexulose 7-Phosphate Synthase from Mycobacterium Tuberculosis: In Silico Screening and in Vitro Validation. *Eur. J. Med. Chem.* **2015**, *105*, 182–193.
- (12) Gibson, F.; Pittard, J. Pathways of Biosynthesis of Aromatic Amino Acids and Vitamins and Their Control in Microorganisms. *Bacteriol. Rev.* **1968**, *32*, 465–492.
- (13) Radaev, S.; Dastidar, P.; Patel, M.; Woodard, R. W.; Gatti, D. L. Structure and Mechanism

- of 3-Deoxy- D - Manno -Octulosonate 8-Phosphate Synthase *. **2000**, 275, 9476–9484.
- (14) Liu, F.; Lee, H. J.; Strynadka, N. C. J.; Tanner, M. E. Inhibition of Neisseria Meningitidis Sialic Acid Synthase by a Tetrahedral Intermediate Analogue. *Biochemistry* **2009**, 48, 9194–9201.
- (15) König, V.; Pfeil, A.; Braus, G. H.; Schneider, T. R. Substrate and Metal Complexes of 3-Deoxy-D-Arabino-Heptulosonate-7- Phosphate Synthase from *Saccharomyces Cerevisiae* Provide New Insights into the Catalytic Mechanism. *J. Mol. Biol.* **2004**, 337, 675–690.
- (16) Shumilin, I. A.; Kretsinger, R. H.; Bauerle, R. H. Crystal Structure of Phenylalanine-Regulated 3-Deoxy-D-Arabino- Heptulosonate-7-Phosphate Synthase from *Escherichia Coli*. *Structure* **1999**, 7, 865–875.
- (17) Rigden, D. J. *From Protein Structure to Function with Bioinformatics: Second Edition*; 2017.
- (18) Yang, L. Q.; Sang, P.; Tao, Y.; Fu, Y. X.; Zhang, K. Q.; Xie, Y. H.; Liu, S. Q. Protein Dynamics and Motions in Relation to Their Functions: Several Case Studies and the Underlying Mechanisms. *J. Biomol. Struct. Dyn.* **2014**, 32, 372–393.
- (19) Karplus, M.; Kuriyan, J. Molecular Dynamics and Protein Function. *Proc. Natl. Acad. Sci.* **2005**, 102, 6679–6685.
- (20) Boehr, D. D.; Dyson, H. J.; Wright, P. E. An NMR Perspective on Enzyme Dynamics. *Chem. Rev.* **2006**, 106, 3055–3079.
- (21) Rob, T.; Liuni, P.; Gill, P. K.; Zhu, S.; Balachandran, N.; Berti, P. J.; Wilson, D. J. Measuring Dynamics in Weakly Structured Regions of Proteins Using Microfluidics-Enabled Subsecond H/D Exchange Mass Spectrometry. *Anal. Chem.* **2012**, 84, 3771–3779.
- (22) Engen, J. R. Analysis of Protein Conformation and Dynamics by Hydrogen / Deuterium Exchange MS. **2009**, 7870–7875.
- (23) Law, W. H.; Berti, P. J. Creating Mutant DAHPS(Tyr) Proteins with Nudge Mutagenesis for the 19F NMR Protein Dynamics Studies, McMaster University, 2016.
- (24) Kitevski-LeBlanc, J. L.; Prosser, R. S. Current Applications Of 19F NMR to Studies of Protein Structure and Dynamics. *Prog. Nucl. Magn. Reson. Spectrosc.* **2012**, 62, 1–33.
- (25) Demeule, B.; Lawrence, M. J.; Drake, A. F.; Gurny, R.; Arvinte, T. Characterization of Protein Aggregation: The Case of a Therapeutic Immunoglobulin. *Biochim. Biophys. Acta - Proteins Proteomics* **2007**, 1774, 146–153.
- (26) Pecora, R. Dynamic Light Scattering Measurement of Nanometer Particles in Liquids. *J. Nanoparticle Res.* **2000**, 2, 123–131.

- (27) Stetefeld, J.; McKenna, S. A.; Patel, T. R. Dynamic Light Scattering: A Practical Guide and Applications in Biomedical Sciences. *Biophys. Rev.* **2016**, *8*, 409–427.
- (28) Li, Y.; Lubchenko, V.; Vekilov, P. G. The Use of Dynamic Light Scattering and Brownian Microscopy to Characterize Protein Aggregation. *Rev. Sci. Instrum.* **2011**, *82*.
- (29) Berne, B. J.; Pecora, R. *Dynamic Light Scattering: With Applications to Chemistry, Biology and Physics*; Dover: Mineola, NY, 2000.
- (30) Meric, G.; Robinson, A. S.; Roberts, C. J. Driving Forces for Nonnative Protein Aggregation and Approaches to Predict Aggregation-Prone Regions. *Annu. Rev. Chem. Biomol. Eng.* **2017**, *8*, 139–159.
- (31) Hamada, H.; Arakawa, T.; Shiraki, K. Effect of Additives on Protein Aggregation. *Curr. Pharm. Biotechnol.* **2009**, *10*, 400–407.
- (32) Furdui, C.; Zhou, L.; Woodard, R. W.; Anderson, K. S. Insights into the Mechanism of 3-Deoxy-D-Arabino-Heptulosonate 7-Phosphate Synthase (Phe) from Escherichia Coli Using a Transient Kinetic Analysis. *J. Biol. Chem.* **2004**, *279*, 45618–45625.
- (33) Yoshida, H.; Hensgens, C. M. H.; Van Der Laan, J. M.; Sutherland, J. D.; Hart, D. J.; Dijkstra, B. W. An Approach to Prevent Aggregation during the Purification and Crystallization of Wild Type Acyl Coenzyme A: Isopenicillin N Acyltransferase from *Penicillium Chrysogenum*. *Protein Expr. Purif.* **2005**, *41*, 61–67.
- (34) Faucher, A.-M.; Grand-Maître, C. Tris (2-Carboxyethyl)Phosphine (TCEP) for the Reduction of Sulfoxides, Sulfonylchlorides, N -Oxides, and Azides . *Synth. Commun.* **2003**, *33*, 3503–3511.
- (35) Golovanov, A. P.; Hautbergue, G. M.; Stuart A. Wilson, S. A.; Lian, L.-Y. A Simple Method for Improving Protein Solubility and Long-Term Stability. *J. Am. Chem. Soc.* **2004**, *126*, 8933–8939.
- (36) Arakawa, T.; Ejima, D.; Tsumoto, K.; Obeyama, N.; Tanaka, Y.; Kita, Y.; Timasheff, S. N. Suppression of Protein Interactions by Arginine: A Proposed Mechanism of the Arginine Effects. *Biophys. Chem.* **2007**, *127*, 1–8.
- (37) Scott, D. E.; Coyne, A. G.; Hudson, S. A.; Abell, C. Fragment-Based Approaches in Drug Discovery and Chemical Biology. *Biochemistry* **2012**, *51*, 4990–5003.
- (38) Harner, M. J.; Frank, A. O.; Fesik, S. W. Fragment-Based Drug Discovery Using NMR Spectroscopy. *J. Biomol. NMR* **2013**, *56*, 65–75.
- (39) O’Shea, R.; Moser, H. E. Physicochemical Properties of Antibacterial Compounds: Implications for Drug Discovery. *J. Med. Chem.* **2008**, *51*, 2871–2878.

- (40) Gama, S. R.; Balachandran, N.; Berti, P. J. Campylobacter Jejuni KDO8P Synthase, Its Inhibition by KDO8P Oxime, and Control of the Residence Time of Slow-Binding Inhibition. *Biochemistry* **2018**, *57*, 5327–5338.
- (41) Popovic, V.; Morrison, E.; Rosanally, A. Z.; Balachandran, N.; Senson, A. W.; Szabla, R.; Junop, M. S.; Berti, P. J. NeuNAc Oxime: A Slow-Binding and Effectively Irreversible Inhibitor of the Sialic Acid Synthase NeuB. *Biochemistry* **2019**, *58*, 4236–4245.
- (42) Heimhalt, M.; Berti, P. J. Mechanisms of Imine-Based Inhibitors of DAHP Synthase. **2017**, 219.
- (43) Shumilin, I. A.; Bauerle, R.; Kretsinger, R. H. The High-Resolution Structure of 3-Deoxy-d-Arabino-Heptulosonate-7-Phosphate Synthase Reveals a Twist in the Plane of Bound Phosphoenolpyruvate. *Biochemistry* **2003**, *42*.
- (44) Chen, J. M.; Xu, S. L.; Wawrzak, Z.; Basarab, G. S.; Jordan, D. B. Structure-Based Design of Potent Inhibitors of Scytalone Dehydratase: Displacement of a Water Molecule from the Active Site. *Biochemistry* **1998**, *37*, 17735–17744.
- (45) Fox, J. D.; Kapust, R. B.; Anderson, D. E.; Cherry, S.; Copeland, T. D.; Waugh, D. S. Tobacco Etch Virus Protease : Mechanism of Autolysis and Rational Design of Stable Mutants with Wild-Type Catalytic Proficiency. **2001**, *14*, 993–1000.
- (46) Lanzetta, P. A.; Alvarez, L. J.; Reinach, P. S.; Candia, O. A. An Improved Assay for Nanomole Amounts of Inorganic Phosphate. *Anal. Biochem.* **1979**, *100*, 95–97.
- (47) Sieben, A. S.; Perlin, A. S.; Simpson, F. J. *Biochemistry*. **1966**, *44*, 2–8.
- (48) Parkin, D. W.; Horensteingn, B. a; Abdulahg, D. R.; Estupiiang, B.; Schrammgii, V. L. Nucleoside Hydrolase from Crithidia Fasciculata. *J. Biol. Chem.* **1991**, *266*, 20658–20665.
- (49) Merck KGaA. Enzymatic Assay of Glucose-6-Phosphate Dehydrogenase <https://www.sigmaaldrich.com/technical-documents/protocols/biology/enzymatic-assay-of-glucose-6-phosphate-dehydrogenase.html>.
- (50) Stickland, S.; Massey, V. The Mechanism of Action of the Flavoprotein Melilotate Hydroxylase. *J. Biol. Chem.* **1973**, *218*, 2953–2962.
- (51) Balachandran, N. DAHP Oxime: A Transition State Mimic Inhibitor Of DAHP Synthase, McMaster University, 2014.
- (52) Duke, C. C.; MacLeod, J. K.; Williams, J. F. Nuclear Magnetic Resonance Studies of D-Erythrose 4-Phosphate in Aqueous Solution. Structures of the Major Contributing Monomeric and Dimeric Forms. *Carbohydr. Res.* **1981**, *95*, 1–26.
- (53) Rosano, G. L.; Ceccarelli, E. A. Recombinant Protein Expression in Escherichia Coli :

Advances and Challenges. **2014**, 5, 1–17.

- (54) Schein, C. H.; Noteborn, M. H. M. Formation of Soluble Recombinant Proteins in Escherichia Coli Is Favored by Lower Growth Temperature. *Nat. Biotechnol.* **1988**.
- (55) Sako, Y.; Nomura, N.; Uchida, A.; Ishida, Y.; Morii, H.; Koga, Y.; Hoaki, T.; Maruyama, T. Aeropyrum Pernix Gen. Nov., Sp. Nov., a Novel Aerobic Hyperthermophilic Archaeon Growing at Temperatures up to 100 C. *Int. J. Syst. Bacteriol.* **1996**, 46, 1070–1077.
- (56) Cui, D.; Deng, A.; Bai, H.; Yang, Z.; Liang, Y.; Liu, Z.; Qiu, Q.; Wang, L.; Liua, S.; Zhanga, Y.; et al. Molecular Basis for Feedback Inhibition of Tyrosine-Regulated 3-Deoxy-D- Arabino-Heptulosonate-7-Phosphate Synthase from Escherichia Coli. *J. Struct. Biol.* **2019**, No. May, 322–334.
- (57) Zhou, L.; Wu, J.; Janakiraman, V.; Shumilin, I. A.; Bauerle, R.; Kretsinger, R. H.; Woodard, R. W. Structure and Characterization of the 3-Deoxy-d-Arabino-Heptulosonate 7-Phosphate Synthase from Aeropyrum Pernix. *Bioorg. Chem.* **2012**, 40, 79–86.